Université de Montréal

Recherche de la raie Hα dans un échantillon de naines blanches chaudes du type DB

par

Chris Hunter

Département de physique

Faculté des arts et des sciences

Mémoire présenté à la Faculté des études supérieures

en vue de l'obtention du grade de

MSc

en physique

Août, 2001

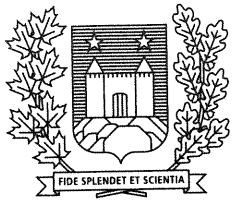

Université de Montréal

Bibliothèque

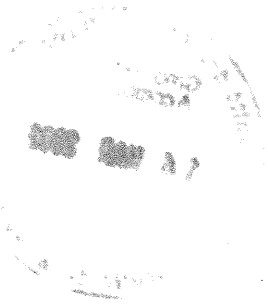

Université de Montréal

Faculté des études supérieures

Ce mémoire intitulé:

Recherche de la raie Hα dans un échantillon de naines blanches chaudes du type DB

présenté par:

Chris Hunter

a été évalué par un jury composé des personnes suivantes:

Gilles Fontaine,	président-rapporteur
Francois Wesemael,	directeur de recherche
Serge Demers,	membre du jury

Mémoire accepté le: _____

Sommaire

Les étoiles naines blanches de type spectral DB sont des objets caractérisés par une atmosphère d'hélium d'une grande pureté. Nous présentons ici les résultats d'une étude visant à déterminer l'abondance résiduelle d'hydrogène dans les atmosphères de ces objets. Nous avons, pour ce faire, observé un échantillon de 26 naines blanches chaudes de type DB. Dans le but d'établir les meilleures contraintes sur l'abondance d'hydrogène, nos observations spectroscopiques couvrent la région rouge du spectre visible (λ5700Å-λ7200Å), qui inclut la transition Hα de l'hydrogène. Nos observations sont ensuite comparées à une grille de spectres synthétiques de cette région spectrale afin d'obtenir l'abondance d'hydrogène pour chaque objet.

Nous trouvons que 38% (7/18) des étoiles chaudes de type DB (classe DB2) montrent la raie Hα, et sont conséquemment membres de la sous-classe DBA2. Ces objets ont une abondance moyenne de log $y\sim$4.0. L'hydrogène y est donc en moyenne 10,000 fois moins abondant que l'hélium. Pour les autres étoiles qui ne montrent pas la raie Hα , et qui demeurent donc de type DB2, nous avons obtenus des limites superieures à l'abondance d'hydrogène dans la photosphère.

Nos résultats sont généralement en accord avec ceux récents de Provencal et al. (2000), en ce que les deux étoiles chaudes PG 0112+104 et GD 358 ont des quantités d'hydrogène photosphérique trop petites pour avoir formé une couche opaque d'hydrogène aux températures typique de la brèche des DB, au-delà de 30,000 K. Une redétermination autocohérente de l'échelle de température des étoiles DB chaudes montre également que la bande d'instabilité des étoiles variables de type DB s'etend entre 28,000K et 21,000K. Les étoiles pulsantes de type DBA semblent concentrées du côté froid de cette bande. Une étoile magnétique et

apparemment constante mise à part, la bande semble ne contenir que des étoiles variables.

Table des matières

Sommaire 1

Table des matières 3

Table des figures 5

Liste des tableaux 7

Introduction 8

1 A search for Hα in Hot DB white dwarfs 12

Abstract . . . 13

1.1 Introduction . . . 13

1.2 Observations . . . 16

1.3 Models . . . 17

1.4 Analysis . . . 19

1.4.1 Fitting Technique . . . 19

1.4.2 Testing new analysis methods: Comparison with previous results . . . 22

1.4.3 Simulations . . . 23

1.5 Results . . . 26

1.5.1 Determination of Atmospheric Parameters . . . 26

1.5.2 Spectra with two solutions . . . 27

1.5.3 Simulation Results . . . 29

1.5.4 Detection Limits . . . 31

1.6 Discussion 33
1.6.1 DBA Fraction 33
1.6.2 Theoretical equivalent widths 34
1.6.3 Temperature scale of pulsating DB white dwarfs 35
1.6.4 DBV Instability Strip 37
1.6.5 Is hydrogen primordial or accreted? 39
1.7 Summary 44
1.8 References 45
1.9 Figures 51

Conclusion **83**

Références **86**

Remerciements **90**

Table des figures

1.1 Comparison of survey sample with DB stars in McCook & Sion Catalog 51

1.2 New red spectra I 52

1.3 New red spectra II 53

1.4 Theoretical equivalent widths of He I lines 54

1.5 Example of pseudo-gaussian fits to synthetic spectra 55

1.6 Compare T_{eff} with Beauchamp et al. (1999) ; DB, no H 56

1.7 Compare log g with Beauchamp et al. (1999); DB, no H 57

1.8 Compare T_{eff} with Beauchamp et al. (1999) ; DBA 58

1.9 Compare log g with Beauchamp et al. (1999); DBA 59

1.10 Compare T_{eff} with Beauchamp et al. (1999) ; DB, H 60

1.11 Compare log g with Beauchamp et al. (1999); DB, H 61

1.12 Blue spectra simulation results for log g 62

1.13 Simulation results for log g example I 62

1.14 Simulation results for log g example II 63

1.15 Two solutions for G 270-124 64

1.16 Two solutions for PG 1445+152 64

1.17 Two solutions for PG 2234+064 65

1.18 Two solutions for PG 2354+159 65

1.19 Simulation of LP 475-242 66

1.20 Simulation of GD 378 66

1.21 Simulation of PG 0129+246 67

1.22 Simulation of GD 61 67

1.23 Simulation of GD 243 68
1.24 Simulation of Feige 4 68
1.25 Simulation of GD 205 69
1.26 Simulation of PG 1456+103 69
1.27 Simulation of PG 0921+091 70
1.28 Simulation of PG 1540+680 70
1.29 Simulation of G 270-124 71
1.30 Simulation of PG 1445+152 71
1.31 Simulation of PG 2234+064 72
1.32 Simulation of PG 2354+159 72
1.33 Simulation of GD 233 73
1.34 Simulation of GD 190 73
1.35 Simulation of GD 198 74
1.36 Simulation of GD 358 74
1.37 Simulation of PG 1654+160 75
1.38 Simulation of PG 2246+120 75
1.39 Simulation of EC20058-5234 76
1.40 Simulation of PG 0112+104 76
1.41 Hydrogen detection limits 77
1.42 Hα limit for PG 0112+104 77
1.43 DBA fraction of DB2 stars 78
1.44 DBA fraction of all current DB spectra 78
1.45 λ7065Å Equivalent Widths 79
1.46 λ4471Å Equivalent Widths 79
1.47 Period-temperature relation of DBV stars 80
1.48 Weighted period-temperature relation 80
1.49 Empirical Instability Strip 81
1.50 Hydrogen masses of DBA stars 82

Liste des tableaux

1.1 Journal of Observations 18

1.2 Comparison with previous results in Beauchamp et al. (1999) 23

1.3 Derived atmospheric parameters of program stars 28

1.4 Difficulties in fitting low S/N red spectra 29

Introduction

Les étoiles de masse intermédiaire ($\sim$1 à 10 $M_{\odot}$) finissent leur vie sous la forme d'une étoile dégénérée appelée naine blanche. Dans cette ultime phase évolutive, 99% de la masse de l'étoile est concentrée dans un noyau dense. Au sein de celui-ci, la tendance à l'effondrement dû à la force gravitationelle est contrebalancée par la pression associée à la dégénéréscence des électrons.

Les naines blanches se distinguent de la plupart des étoiles de la séquence principale par le fait qu'il n'y a plus de fusion nucléaire dans leurs régions centrales. Ainsi donc, durant la majorité de sa vie, une naine blanche ne fait que se refroidir, et son énergie thermique s'échappe lentement de l'intérieur. Puisqu'aucun processus ne peut remplacer cette perte d'énergie, le destin de cet objet sera d'atteindre un équilibre à la température de l'Univers.

Au-dessus du noyau se trouve une enveloppe stellaire, elle même entourée d'une atmosphère non-dégénérée. Malgré sa faible masse, l'atmosphère est la seule portion de la naine blanche que nous pouvons observer directement. Cet ensemble de couches externes contrôle le taux de refroidissement des étoiles dégénérées. Il est donc essentiel d'avoir une bonne connaissance des propriétés physiques de ces couches externes afin de déterminer les âges de ces étoiles(voir Hansen (1999); Fontaine et al. (2001) pour des revues récentes).

À partir d'observations spectroscopiques, nous avons identifié divers éléments chimiques dans les atmosphères de naines blanches. Environ 20% des naines blanches sont classifiées spectroscopiquement dans la famille des étoiles dégénérées de type "non-DA" (Sion et al. 1983; McCook & Sion 1999). La plupart de ces étoiles non-DA sont caractérisées par une atmosphère riche en l'hélium.

Une sous-classe des étoiles non-DA, les étoiles DB, correspond à un type spectral ca-

ractérisé par des raies d'hélium neutre aux longueurs d'ondes du visible. Les étoiles de type DB existent sur une gamme de température effective entre 10,000K et 30,000 K. Aux températures effectives inférieures à 10,000 K, les atomes d'hélium ne sont pas excités en nombre suffisant pour produire des raies d'absorption. À haute température effective, les raies d'hélium neutre sont visibles jusqu'à 45,000K. Cependant, aucune étoile de type DB n'a été decouverte avec une température plus élévée que 30,000K. Cette absence d'étoiles chaudes de type DB est connue sous le nom de brèche des DB (Liebert 1986).

La question de la survie des étoiles DB a été posée peu après leur découverte. On suppose qu'elles ont rencontré, dans la Galaxie, des régions plus denses du milieu interstellaire (ISM) (Wesemael 1979) pendant les quelques milliards d'années que dure leur vie. Il est donc difficile d'expliquer pourquoi ces naine blanches n'ont pas accumulé de ce fait une quantité suffisante d'hydrogène pour être recouverte d'une pellicule opaque de cet élément. Une masse minimale de $M_H = 10^{-16} M_\odot$, acquise par accrétion de matière solaire dans le milieu interstellaire, serait suffisante pour transformer une étoile de type DB en une étoile de type spectral DA, à atmosphère d'hydrogène (D'Antona & Mazzitelli 1979). Plusieurs études ont suggéré que ce type d'accrétion pourrait être inhibé (par example, via une interaction avec le champ magnetique stellaire (Wesemael & Truran 1982)), ou que l'hydrogène accrété pourrait être détruit par combustion nucléaire residuelle (Michaud et al. 1984). Le problème de l'existence des étoiles DB reste cependant entier.

Quelques étoiles naines blanches de type DB ont de petites quantités d'hydrogène dans leur photosphère (Wickramasinghe & Whelan 1977; Shipman et al. 1987), et sont alors classifiées DBA. La découverte des étoiles de type DBA indique peut-être que quelques-unes des étoiles de type DB auraient accreté de l'hydrogène du milieu interstellaire. Une autre évidence provient de la détection de raies de métaux comme le calcium dans le spectre d'étoiles DB. Parce que le tri gravitationnel fait disparaître les métaux sous la photosphère en une courte periode de temps, le calcium doit être périodiquement réapprovisionné afin de rester présent en surface.

La population relative d'étoiles de types DO (caractérisées par des raies d'hélium ionisé) et DB soutient l'hypothèse que les naines blanches de type DO sont les progéniteurs des étoiles DB (Wesemael et al. 1985). À cause de l'existence d'une brèche entre les étoiles DO, plus

chaudes, et les DB, il a été suggéré que les DO se transforment en naines blanches de type DA dans l'intervalle de 45,000 K à 30,000 K. À 30,000 K, elles retrouveraient une atmosphère d'hélium et redeviendraient des DB.

Liebert et al. (1987) ont presenté un scénario de ce type, où le tri gravitationnel force l'hydrogène à monter vers la surface dans les étoiles de type DO. Quand une étoile non-DA atteint la température de 45,000K, la quantité d'hydrogène à la photosphère est alors suffisante pour qu'une couche opaque d'hydrogène se soit formée. L'étoile apparaît donc comme une naine blanche de type DA, à atmosphère riche en hydrogène. À plus faible température effective, vers 30,000 K, la réapparition des raies d'helium neutre coinciderait avec le moment où la zone convective transporte une fraction importante du flux dans l'enveloppe. La mince couche superficielle d'hydrogène pourrait alors être diluée dans la zone convective d'hélium, elle même beaucoup plus massive. Ce phénomène de dilution diminuerait alors l'abondance d'hydrogène en surface sous le seuil de détection, et l'étoile se présenterait maintenant sous l'aspect d'une étoile de type DB. Ce scénario concordait initialement très bien avec les observations (Pelletier et al. 1989). Aujourd'hui, certaines observations qui décèlent la présence d'hydrogène dans les étoiles chaudes ($\sim$100,000K) de type PG1159 représentent un défi pour ce modèle.

L'astrophysicien est constamment à la recherche de méthodes indirectes qui permettraient de "voir" les processus physiques, tel le mélange convectif, qui opèrent sous la photosphère. La séismologie stellaire, ou astéreoséismologie, est une des techniques qui nous permet de déduire les conditions physiques dans l'enveloppe des étoiles pulsantes de type DB (ou étoiles DB variables, DBV). Pour ces étoiles, l'astéreoséismologie a déjà demontré son potentiel dans nos études des propriétés physiques de l'enveloppe (Bradley et al. 1993) et peut-être aussi du noyau (Metcalfe et al. 2000). Les luminosités des modèles astéroséismologiques sont calibrées à l'aide des températures et gravités de surface fournies par la spectroscopie. Il nous faut donc utiliser les meilleures theories d'élargissement des raies et des observations de haute qualité afin de procéder à une calibration fiable des résultats astroséismologiques.

Beauchamp (1995) a récemment fait une mise du jour des modèles d'atmosphères des étoiles de type DB. Il a également étudié les effets d'une trace d'hydrogène dans l'atmosphère

sur les températures effectives déterminées pour les étoiles DB chaudes. Il conclut que de faibles quantités d'hydrogène, à peine visibles du point de vue spectroscopique, pourraient avoir une influence significative sur les températures effectives déterminées pour les étoiles DB les plus chaudes, un échantillon qui inclut toutes les étoiles pulsantes de ce type (Beauchamp et al. 1999). Il importe, donc, de bien connaître la quantité d'hydrogène présente dans les photosphères des étoiles DB les plus chaudes. Dans le cadre de ce Mémoire, nous avons observé toutes les étoiles DB chaudes connues dans l'hemisphère nord dans le but de détecter dans leur spectre la raie de Balmer Hα. Les premiers résultats de cette recherche ont été présentés par Hunter et al. (2001). Le présent travail, plus élaboré, vise maintenant à répondre aux questions suivantes:

1. Est-ce que la présence d'hydrogène a un effet sur les paramètres déterminés pour les étoiles DB pulsantes? Quand on tient compte de l'influence de traces d'hydrogène sur la structure atmosphérique et sur les spectres de naines blanches de type DBV, la structure de la bande d'instabilité est-elle changée? Au sein de la bande d'instabilité, est-ce que l'on peut distinguer les DB non-pulsantes (s'il y en a) des pulsantes par la composition chimique de leur atmosphère?
2. Est-ce qu'il y a de l'évidence d'accrétion d'hydrogène en provenance du milieu interstellaire sur les étoiles DB chaudes? L'abondance d'hydrogène augmente-elle au fur et à mesure que les étoiles refroidissent?
3. Est-ce que les naines blanches de type DBA représentent vraiment une classe spectroscopique distincte des étoiles de type DB? Ou alors, comme plusieurs l'ont déjà suggéré, est-ce que toutes les naines blanches DB contiennent de petites quantités d'hydrogène ?

Chapitre 1

A Search for Hα in a Sample of Hot DB White Dwarfs

C. Hunter [1], F. Wesemael [1], R. Saffer [2], P. Bergeron [1], A. Beauchamp [1]

Received _____; accepted _____

For submission to the ApJ

[1]Département de Physique, Université de Montréal,

C.P. 6128 Succursale Centre-Ville, Montréal, Québec H3C 3J7, Canada

[2]Department of Astronomy and Astrophysics, Villanova University,Villanova, PA 19085

Abstract

We have investigated the effect of hydrogen in the spectra of 26 helium-atmosphere hot DB white dwarfs. Our sample uses Hα to constrain hydrogen abundances using new model atmospheres, which include the red portion of the optical spectrum (λ5700Å-λ7200Å). We find roughly 38% (7/18) of the DB2 stars in this survey show a visible Balmer line in their spectra and belong to the DBA2 subtype. The DBA2 objects have an average abundance ratio of log y~4.0.

For the remaining objects, we derive upper limits for photospheric hydrogen abundances. Our results agree with recent work from Provencal et al. (2000) that for the two stars PG 0112+104 and GD 358 the upper limit of photospheric hydrogen mass is too small to explain the "DB gap" by chemical diffusion of hydrogen forming an opaque surface layer at the representative effective temperature.

We estimate the empirical instability strip for DB variables extends over the temperature range of 28,000K to 21,000K. The cool end of the instability strip is occupied by the DBA pulsating stars in our sample. We suggest that this empirical instability strip does not contain any non-magnetic non-pulsating stars.

1.1 Introduction

White dwarfs are the remnants of main sequence stars that have exhausted their nuclear energy source. Internally, a white dwarf most likely has a quiescent degenerate carbon/oxygen core. After a few 10^7 years, the core does not appreciably change in composition. However, the thin non-degenerate envelope (less than 1% of total white dwarf mass) undergoes significant chemical upheaval. As this envelope controls the cooling rate of older white dwarfs, understanding chemical evolution in white dwarfs is critical in assigning cooling ages (Fontaine et al. 2001). Observations have allowed us to identify many different chemical species present in the photospheres of white dwarfs. Approximately 20% of all spectroscopically identified white dwarfs are part of the family of non-DA degenerate stars (Sion et al. 1983; McCook & Sion 1999). The majority of non-DAs have helium as the dominant atmospheric constituent.

DB white dwarfs belong to the non-DA spectroscopic class identified by broad He I absorption lines at optical wavelengths. DB stars exist over effective temperatures 10,000K - 30,000K. At cooler temperatures, the helium atom is no longer excited in sufficient numbers to produce absorption lines. Although neutral helium lines are expected to be visible up to surface temperatures of 45,000K, no DB star has ever been discovered above 30,000K, This lack of DB stars at higher effective temperatures is known as the 'DB gap' (Liebert 1986) and is perhaps one of the best observational clues that white dwarfs undergo chemical evolution during their long cooling lifetimes.

Shortly after their discovery, the question was raised as to why white dwarfs with helium atmospheres exist at all (Eggen & Greenstein 1965). Some of these stars have orbited our Galaxy for $\gtrsim 5\ Gyr$. In this time they have presumably encountered dense regions of the interstellar medium and giant molecular clouds (Wesemael 1979; Aannestad & Sion 1985; Dupuis et al. 1987). It is difficult to explain why these stars have not trapped sufficient hydrogen in their gravitational wells to form an opaque surface layer of hydrogen. Only a minuscule amount ($10^{-16} M_{\odot}$) is necessary by accretion of solar composition material (D'Antona & Mazzitelli 1979). To explain the lack of hydrogen in the photosphere, physical mechanisms have been suggested to either inhibit accretion, such as interaction with a stellar magnetic field (Wesemael & Truran 1982) or to destroy accreted hydrogen by diffusive burning (Michaud et al. 1984).

Some DB white dwarfs were discovered to contain trace amounts of hydrogen (Wickramasinghe & Whelan 1977; Shipman et al. 1987, hereafter SLG87) and were subsequently labeled as spectral type DBA. The discovery of DBA stars may indicate that at least some white dwarfs are accreting material from the interstellar medium (ISM)–further evidence comes from the discovery of Ca II lines in the spectra of a few DBAs (Wickramasinghe et al. 1975; Koester & Wolff 2000). Heavy elements rapidly sink in white dwarf atmospheres. The short lifetime of calcium in white dwarf photospheres means metals must occasionally be renewed at the surface.

The discovery of the "DB gap" between hot He II-line DO and He I-line DB stars led to the realization that non-DA white dwarfs may not be as distinct from DAs as originally

believed. To explain the lack of non-DAs with temperatures between 45,000 and 30,000K, it is generally argued that DO white dwarfs "evolve" into DA stars and then are restored to a helium atmosphere to become DB white dwarfs. The relative number of DO and DB stars lends itself to DO stars being the progenitors of DB degenerates (Wesemael et al. 1985).

The single (evolutionary) channel "float-up" scenario was introduced to explain the observational evidence, such as the ratio of non-DA to DA white dwarfs (Sion 1984), for the chemical evolution of non-DAs white dwarfs (Liebert et al. 1987). Due to the strong surface gravities, hydrogen will "float" above all heavier elements in the atmospheres of degenerate stars. Even if a white dwarf started with a turbulently mixed atmosphere, the elements will separate (heavier helium and metals would sink while hydrogen would rise) after only a few centuries (Pelletier et al. 1989). However, the recent discovery of hydrogen in hot (~100,000K) "pre-white dwarfs" (PG1159 stars) (Napiwotzki 1999), which are thought of as the precursors to *all* white dwarfs, has raised questions about the validity of this scenario.

Spectroscopy does not allow us to probe beneath the photosphere into deeper portions of white dwarfs atmospheres, where most of the evolution occurs. The discovery of pulsating V777 Her or DBV stars has allowed us to infer the physical properties below regions seen by spectroscopy. Astereoseismology has shown potential to investigate envelope (Bradley et al. 1993, hereafter BWW93) and possibly core properties (Metcalfe et al. 2000) of pulsating white dwarfs. Since astereoseismological luminosities are "calibrated" to estimates of temperature and mass provided from spectroscopy, high quality observations and the most current line-formation theory must be used for reliable seismological results.

Following a recent overhaul of DB atmosphere modeling (Beauchamp et al. 1995b) it was realized that trace amounts of hydrogen can cause significant change in the spectroscopic temperatures of hot DB stars (Beauchamp et al. 1999, hereafter B99). As the previous survey of DBA stars in SLG87 focused on lower temperatures ($T_{\rm eff}$ < 19,000K), we undertook to observe all hot DB2 and several DB3 white dwarfs for trace hydrogen through measurement of Hα absorption. Preliminary discussion of our results were presented by Hunter et al. (2001, hereafter HWSBB01).

We outline three topics we wish to explore with this paper:

1. What is the effect of hydrogen on DBV stars ? Does it change the boundaries or structure of the empirical "instability strip" (temperature range which bounds all known DBVs) ? Can we explain the non-pulsating DB stars inside the strip by atmospheric composition ?

2. Do hot DB stars show evidence of accretion from the ISM (molecular clouds) ? For example, does hydrogen abundance increase with the cooling age of these stars ?

3. Can we confirm the statement that "All DBs probably contain H as a trace constituent" (Koester & Weidemann 1989), i.e, is the DBA spectral type the rule rather than the exception for DB stars ?

We briefly discuss the new observations for this study in section 1.2 and models in section 1.3. Discussion of the analysis methods and comparison with other results previously reported by our group are presented in sections 1.4.1-1.4.3. Results derived from spectra are presented in sec. 1.5.1-1.5.4. Section 1.6 compares our results with previous work. Sections 1.6.3 and 1.6.4 discuss how our new study reflects upon white dwarf astereoseismology. In section 1.6.5 we estimate hydrogen masses for DBA stars in the context of accretion of hydrogen in DB white dwarfs1.

1.2 Observations

As part of an ongoing campaign to observe all bright northern DB stars in the McCook & Sion Catalog, a sub-sample that delineates the variable DB instability strip was studied in B99. From this study, the importance of constraining hydrogen abundance was recognized. The stars discussed in this paper were culled mostly on the basis of the absence of an Hβ line, so Hα is needed to limit further the hydrogen content. Some cooler stars were included to provide continuity and allow comparison with previous work on DBA stars.

We focused our observations mostly on white dwarfs hotter than the DBA stars discovered in the PG survey (Green et al. 1986, SLG87). The histogram in figure 1.1 plots our sample compared to all DB stars listed in the McCook & Sion catalog as a function of effective temperature. For this figure, we have used the final temperatures presented in this article

and binned the results into half-integer bins, as suggested in McCook & Sion (1999). We have secured blue and red spectra for all the hot stars listed as DB2 in the catalog, as well as a few cooler DBA3 stars. We also include the southern DBV EC20058-5234 in our analysis (observations described in B99). In addition to the sensitivity problems below 4100Å discussed in B99, the spectrum of EC20058-5234 also has similar difficulties above 6800Å. We restrict our analysis of this star to the range between these wavelengths.

Observations of Hα were conducted with the 4m telescope at KPNO in 1999 and early 2000. The instrumental setup used the 4m Ritchey-Chretien Spectrograph with a Tektronix 2kx2k CCD. A grating with 790 lines/mm blazed at 9500Å was used in first order. Slit width varied between 1.5″ and 3″. This setup provided a spectra coverage of 5700 to 7200Å with a FWHM∼3 Å. The resulting S/N ratio ranges from 20 to 100. Due to an error in the grating tilt, some of the spectra on the first night only cover 5800-7200Å and provide only partial coverage of the He I λ5876 profile.

Instrumental setup for the blue DB spectra acquired earlier was described in B99. These follow closely the observations of DA stars (Bergeron et al. 1992, 1995). The spectra were taken at the 2.3m Steward Observatory, cover the range 3700-5100Å with a FWHM ∼6Å. The resulting S/N ratio varies between ∼50 and 80.

Table 1.1 lists our table of observations. Figures 1.2 and 1.3 shows our new red spectra as well as the red portion of EC20058-5234 and the blue spectrum for PG 1654+160.

1.3 Models

Synthetic spectra for the wavelength regions in this study are the result of PhD work by A. Beauchamp (Beauchamp 1995). These include significant improvements in line broadening calculations as well as the inclusion of many resolved and unresolved forbidden components. For the hotter stars, the effect of both quadratic and linear Stark broadening of He I lines are included. New tables of broadening coefficients were computed to replace outdated values. These changes resulted in significant improvement in the short-wavelength lines and line wings of all optical profiles..

Journal of Observations

WD	Name	Ordinal	Date (UT)	Exposure Time (s)	Dominant Period (s)	V
0017+136	Feige 4		1999 Sep 30	1270		15.2
0100-068	G 270-124		1999 Sep 30	600		13.8
0112+104	PG 0112+104		2000 Feb 25	2120		15.4
0129+247	PG 0129+247		1999 Sep 30	2545		16.1pg
0435+410	GD 61		1999 Sep 30	1200		14.9
0437+138	LP 475-242		2000 Feb 24	1270		14.8
0513+260	KUV05134+2605	1	2000 Feb 23	2845	700	16.3
0921+092	PG 0921+092		2000 Feb 23	3600		16.2pg
0954+342	CBS 114	2	2000 Feb 23	4410	650	17pg
1115+158	PG 1115+158	3	2000 Feb 23	3120	1000	16.1pg
1351+489	PG 1351+489	4	2000 Feb 25	3120	490	16.4pg
1445+152	PG 1445+152		2000 Feb 23	2545		14.6pg
1456+130	PG 1456+103	5	2000 Feb 23	1700	660	15.9pg
1540+680	PG 1540+680		2000 Feb 25	2545		16.6pg
1542+182	GD 190		2000 Feb 23	900		14.6
1612-111	GD 198		2000 Feb 23	1275		15.5
1645+325	GD 358	6	1999 Sep 30	600	700	14.0
1709+230	GD 205		2000 Feb 23	850		15.0
1822+410	GD 378		1999 Sep 30	660		14.0
2130-047	GD 233		1999 Sep 30	810		14.5
2234+064	PG 2234+064		1999 Sep 30	1800		15.8pg
2246+121	PG 2246+121	9	1999 Sep 30	3120	330	16.2pg
2253-062	GD 243		1999 Sep 30	1275		15.5pg
2354+159	PG 2354+159		1999 Sep 30	1700		15.8pg
1654+160	PG 1654+160	7	1995 Jul 16		580	16.2pg
2009-524	EC20058-5234	8			260	15.5

Table 1.1: Journal of observations of the red spectra. For PG 1654+160, the date refers to acquisition of the blue spectrum (λ3700-5100) as no Hα coverage is currently available. The DBV EC20058-5234 is treated separately due to instrumental problems. Visual magnitudes are multichannel or photographic (denoted by the "pg" suffix) measurements. Numbering of DB variables, in the "Ordinal" column, follows B99 with PG 2246+120 (Handler 2001) assigned #9. Exposure times are the sum of squares of co-added spectra. Periods listed are dominant periods for multi-periodic objects are described in section 1.6.3

New LTE atmosphere models use the Hummer-Mihalas (Hummer & Mihalas 1988) occupation probability formalism for the equation of state. Convection mixing length for these models was chosen to give the best agreement between IUE UV observations and ground-based spectroscopy as discussed in Beauchamp (1995). Pseudo-continuum opacity uses the treatment discussed in Dappen et al. (1987).

Details of model atmospheres are presented in Beauchamp et al. (1995a,b, 1996) and Beauchamp et al. (1997). The model grid used here covers $T_{\rm eff} = 16,000{\rm K} - 32,000{\rm K}$, $\log g = 7.5(0.5)9.0$ ($\rm g \cdot cm/s^2$), and $\log$ *N(He)/N(H)* $= 2.5(0.5)5.5$. Our work represents the first time the red region of DB spectra has been considered in detail. Previously Beauchamp et al. (1995a) used red spectra to identify the forbidden components only. They did not discuss temperatures and gravities derived from the red regions in this article.

As was discussed in Beauchamp et al. (1996) line profiles in hot DB stars are much less sensitive to $T_{\rm eff}$ than in cooler DBs. We see in figure 1.4 that the equivalent width of most He I lines reaches a broad maximum near 22,000K with little change in equivalent width at higher temperatures. Interestingly, the equivalent width of the longer wavelength lines (family of transitions between n=2 and n=3 atomic levels) shows the most temperature dependence. However the small intrinsic width of these lines means they will be more sensitive to noise than the larger overlapping lines in the blue portion of the optical spectra. The reverse behaviour holds true for the dependence on surface gravities; the blue wavelengths are more sensitive than red. Beauchamp (1995) lists the most gravity-sensitive lines as λ3705,3805 as well as the trio of overlapping lines λ4121,4144,4169.

1.4 Analysis

1.4.1 Fitting Technique

Previous analyses of DB spectra used a fitting technique that proved successful for DA white dwarfs (Bergeron et al. 1992, hereafter BSL92). This method uses the Levenberg-Marquardt non-linear least-squares method to derive simultaneously temperature, gravity and hydrogen abundances by fitting models to observed spectra. This method proved successful in deriving

surface gravities and temperatures in DB stars when used with blue spectra (Beauchamp 1995).

Derived values using this code with the red spectra differ significantly compared with results from blue spectra. These discrepancies are caused by the methods used to reduce observations and models to a format where they can be directly compared. The requirements of these reductions are different for the red region than the blue.

Several modifications were necessary for this fitting technique to provide agreement between the two spectral regions. Some of these changes include: i) Ignoring sections of spectra contaminated by telluric absorption: regions between 6270Å and 6400Å and 6860Å and 7000Å were discarded from our fits. This included part of the blue wing of the He I λ7065 line. ii) Combination of blue and red spectra: blue and red spectra were used together for least-squares fitting. Flux normalization of the combined spectra proved difficult. The fluxes at the ends of the individual spectra tend to diverge due to decreasing instrumentation sensitivity. Several red spectra are missing the blue wing of the λ5876 line. For these stars, the left end of the red spectra terminates within an absorption profile. Connecting them by vertically shifting the red spectra to match the fluxes of the last few blue pixels caused fluxes in the rest of the red spectra to be systematically offset.

Changes to the interpolation routines were implemented. Parts of the old code were not re-used. These excluded portions mostly deal with correction of wavelengths by shifting the observed spectra to a laboratory wavelength scale. The new version of the fitting program used here is more flexible, as it can deal with multiple data sets but we sacrificed the accuracy that previous studies obtained from considering only blue spectra of uniform quality.

All fluxes were converted to energy per specific wavelength (H_λ). Observed spectra were shifted to a laboratory wavelength scale (λ_o) by measuring the central wavelengths (λ_c) of each profile separately and then applying the average difference ($< \Delta\lambda >= \frac{\sum_i^N (\lambda_{o_i} - \lambda_{c_i})}{N}$) to the entire spectra. To match the instrumental resolutions of both blue and red data sets, models were convolved with a gaussian at FWHM=6Å for $\lambda < 5600$Å and FWHM=3Å for $\lambda > 5600$Å.

Since our DB spectra have been collected over several observing runs with differing instru-

mental setups and under varying conditions, the spectrophotometry is not uniform. As with the DA spectra in BSL92, our first step is to normalize the line fluxes of both models and observed spectra to a continuum set to unity. Normalization is accomplished by interpolating continuum flux levels, from points chosen in the line-free parts, over the intervening absorption profile. The points used for normalization were chosen interactively for each spectrum. This manual step, not required for DA stars, was necessary because of changes to the continuum regions between cool and hot stars and to allow for adjustments for DBZ stars to avoid the Ca II absorption near λ3930. We averaged the monochromatic fluxes over a few pixels centered around each continuum point. Absorption profiles are normalized by a pseudo-continuum interpolated between the continuum points using cubic splines.

This normalization step is more difficult for DB spectra than for DA spectra. Since He I lines dominate the blue spectra, there are only small line-free regions from where we can extrapolate the continuum. In the red, we are essentially obtaining all temperature and gravity information from three profiles (λ5876, λ6632, λ7065). Of these three profiles we have already lost part of the blue wing of the λ7065 line to telluric absorption. Several spectra only have half the λ5876 profile. The noisier red spectra show poor results for extraction of the continuum fluxes. This poor extraction caused problems with consistent determination of atmospheric parameters between red and blue spectra (discussed in section 1.5.1). We find that the surface gravity is the most sensitive to the results of the continuum extraction.

Bergeron et al. (1995) has since improved on this normalization technique by using pseudo-gaussian profiles (Saffer et al. 1988) as a smooth function to extract Balmer lines from DA spectra. This method proved unsuitable for DB spectra because of three reasons: i) Many He I profiles contain unresolved components and the resulting profile is non-symmetrical. Pseudo-gaussian and pseudo-lorentzian forms assume symmetric line profiles. ii) The He I lines overlap which means we must use overlapping pseudo-gaussians. In practice, small variations in the synthetic spectra would cause one pseudo-gaussian to dominate the combined profile when equal contributions from the two profiles are desired. iii) Pseudo-gaussians do not appear to describe adequately the line wings in hot stars (Fig. 1.5). This could arise from the transition of quadratic to linear Stark broadening changing the wing shape. In addition, we

must simultaneously fit many more lines than DA spectra, which requires higher computing resources.

1.4.2 Testing new analysis methods: Comparison with previous results

Our first order of business is to compare results from the new fitting technique here to those from previous analyses in B99 and HWSBB01. To do this, we repeat the analysis of B99: first we fit only the blue spectra using models containing a hydrogen abundance below our detection threshold (log y=5.5) to compare with the first column of Table 1 (DB, no H) in B99 (Figs. 1.6 and 1.7). This amount of hydrogen is essentially undetectable by Hβ and thus is our approximation to the pure helium model atmospheres used in column 1 of B99. On theoretical grounds, we can expect the mixed H/He atmospheres to be cooler than pure helium. With the hydrogen ratio we have chosen, this difference should be smaller than the uncertainties of our fits. We chose this compromise in order to have all results presented here interpolated from the same model grid (instead of using pure He model atmospheres of B99). Second, we compare results for the five strong-lined Hβ DBA stars where hydrogen abundance is a free parameter in our least-squares fits (figs. 1.8 and 1.9). Finally, we fit blue DB spectra assuming the fixed hydrogen content as described in B99 (DB, H) (figs. 1.10 and 1.11). The amount of hydrogen would produce a barely observable Hβ profile. Note that we do not use the red spectra in this exercise.

As can be seen, there is clearly disagreement between the two studies. Figure 1.6 indicates that we derive systematically higher effective temperatures for stars in the range $T_{\rm eff} \lesssim$ 26,000K. GD 205 appears an exception to the general behaviour, our new code fits this star with $T_{\rm eff}$=21,000K, 3000K less than listed in the first column of B99.

Unusual behaviour is also seen in figure 1.10 where we assume all blue spectra are DBA objects with barely detectable Hβ profiles. There is relatively good agreement for $T_{\rm eff} \gtrsim$ 23,000K. Below this however, our new code fits $T_{\rm eff} \approx$22,000K for almost all stars with temperatures $\leq$22,000K in the third column (DB, H) of B99. This behaviour is related to He I lines reaching maximum strength near this temperature. For cooler stars ($< 20,000$K) our results follow closely with the Beauchamp et al. (1996) and B99.

Comparison of blue spectra fits with Beauchamp et al. (1999)

Column	$\Delta T_{\rm eff} = T_{\rm new} - T_{\rm B99}$	$\sigma_{T_{\rm eff}}$	$\Delta \log g = \log g_{new} - \log g_{B99}$	$\sigma_{\log g}$
DB, no H	510	260	−0.04	0.02
DBA	−290	220	−0.06	0.03
DB, H	220	77	−0.04	0.03

Table 1.2: Summary statistics for figures 1.6 - 1.10 and figures 1.7 - 1.11. We find systematic differences between the two analyses due to the modified fitting technique used here.

We are currently unable to trace the exact cause of these discrepancies. They are possibly due to our new flux normalization routines or to the method used in our code to interpolate between model grid points. The existence of two solutions for some stars is presented in sec. 1.5.2. Further investigation will be required to resolve this issue. In table 1.2 we present the summary statistics between the two studies shown in figures 1.6 - 1.11. These differences should be kept in mind when considering results presented in this paper.

Figures 1.7, 1.9, and 1.11 compare surface gravities. Our new fits consistently give lower log g values (∼0.05 dex). An exceptional case is EC20058-5234 where we find a higher gravity of log g=8.01 compared to log g=7.80 in figure 1.11. We note that the variation in results does not seriously affect the conclusions in Beauchamp et al. (1996): the average mass of DB stars being similar to their DA counterparts. The majority of spectra analyzed for that article are cooler DB stars where we have good agreement with their surface gravities.

1.4.3 Simulations

Error estimates in B99 used the formal co-variance matrix from the least-squares fit. This error is only useful in the case where the rms deviation of the fit is dominated by observation (gaussian) noise. This situation can be compromised in cases where there is a strong dependence between the parameters which affect the final values. Errors derived from the co-variance matrix used by BSL92, upon which the least-squares fitting code in HWSBB01 was based, assume that the atmospheric parameters are independent i.e., the non-diagonal matrix components are much smaller than the diagonal terms (Press et al. 1989). These non-diagonal terms are important as they tell us about interdependence of model parameters.

If the non-diagonal values are significant, we must search for other methods to describe parameter uncertainties. In this regard, the errors discussed in B99 are suspect. They clearly demonstrate a relation between decreasing T_{eff} and increasing hydrogen abundance yet the quoted errors assume these two parameters to be independent.

Given the variations of the temperatures and gravities presented in table 1.3 with those presented in B99, we would like to investigate how different analysis methods affect the quality of our results. Ideally we want to check against our new method causing skewed results, as well as providing estimates of the uncertainty caused by random measurement noise.

We chose the Monte Carlo approach to determine the reliability of our results. We created sets of artificial spectra and treated them as we do real observations in our analysis. We consider this approach an improvement over errors derived from the co-variance matrix.

Artificial data created with known model parameters are an independent method to check our fitting programs for bugs. We can ensure the fits "recover" the simulated values within a certain volume of parameter space centered on the original values. If the results are not centered, this would indicate a systematic effect in our analysis method. Likewise, the volume of parameter space the simulations occupy can be used as an error estimate. More detailed descriptions of parameter space can be provided by drawing contours instead of assuming symmetric error bars. Contours can be used to show parameter dependencies.

The artificial observations were created by extracting spectra from the model grid. To simulate noise, each pixel was multiplied by a gaussian-distributed random variable. The standard deviation of the gaussian was set to the S/N ratio of the real spectrum. Since the blue spectra are fairly uniform in quality, we created artificial spectra with a representative S/N=65 for $\lambda < 5600$ Å. The red portion of the simulated spectra were matched to the S/N ratio of spectra listed in table 1.1.

In stars where we do not see Hα, we need to establish an upper limit of hydrogen content. This involves quantifying the sensitivity of observed spectra to the Hα line strength. The co-variance matrix contains no information about upper limits. For Hβ in B99, this was done by examining each spectrum by eye. With the range of spectral quality for Hα this is a much more subjective and difficult task. We match the S/N ratio of simulated data sets to real

spectra to establish upper limits for all objects in a consistent manner.

Additional simulations were performed with a fixed S/N ratio to establish the visibility limit of Hα as a function of hydrogen abundance. These artificial spectra do not include the effects of telluric absorption. We allowed extrapolated solutions to a value of $N(He)/N(H) \leq 10^{6.0}$ using a simple linear extrapolation beyond our grid boundaries. Any solutions with log y greater than this value were considered to have diverged and the results of that fit were discarded.

Upper limits for non-detection of Hα were determined as follows: for a given set of S/N ratio, T_{eff} and log g values representing a particular object, we would generate a large set of artificial spectra with a fixed $N(He)/N(H)$ ratio. These spectra were then fit in the normal manner like the observed spectra. For large $N(He)/N(H)$ values (small hydrogen content), most of the simulations would return abundance ratios extrapolated beyond our chosen boundary of $N(He)/N(H) \leq 10^{6.0}$. This was interpreted as a $N(He)/N(H)$ ratio below our detection limit. The hydrogen abundance in the artificial spectra was then incrementally increased and the simulations re-run until the non-linear fits returned $N(He)/N(H) \leq 10^{6.0}$ for all the simulated spectra. The fitted points would generally be centered around our simulated $N(He)/N(H)$ value with some scatter dependent on the noise of the artificial spectra.

This method should not be considered rigorous for cool DB stars ($\lesssim 18,000K$), Hα is still visible at $N(He)/N(H) = 10^{6.0}$; this lower limit reflects the finite extent of our model grid. As all cool stars in our sample are DBA sub-types with detectable Hα lines, this is not a critical issue in our analysis.

A second approach was used to test these limits, by inspecting the dispersion(scatter) of simulation results. Using artificial spectra with a fixed hydrogen abundances too small to be detected (e.g. $N(He)/N(H) = 10^{5.5}$) and not worrying about extrapolated values, the smallest log y values returned by simulation fits reflects the largest Hα equivalent width that can be mimicked by noise in a spectrum. In all cases the two methods for estimating upper limits agreed within log y=±0.2 dex.

1.5 Results

1.5.1 Determination of Atmospheric Parameters

We report T_{eff}, log g and log(N(He)/N(H))=log y for all program objects in table 1.3. Recorded values are derived from our non-linear fits. Associated confidence limits are the results of our simulations. The quoted limits for T_{eff} and log y represent the 68% confidence region on the T_{eff}-log y parameter plane. This region contains 68% of the total simulated probability distribution of the parameters. In section 1.5.3, we outline how the distribution is estimated.

During the simulations we discovered that our analysis introduces a systematic bias to derived values of surface gravity. For hot stars ($T_{eff} \gtrsim 21,000K$) we find the mean value of log g as derived from our simulations differs by approximately -0.04 dex from the known value for the synthetic spectra extracted from our models.

Figure 1.12 shows the histogram of values from simulated blue spectra with log g=8.0 and added random noise. There is a tail in the distribution towards lower gravity. The tail moves the mean of the distribution by -0.04 dex. This tail is the most likely explanation for the difference in mean surface gravities in table 1.2. Thus, our gravities in figures 1.7 and 1.11 suffer from a bias introduced during our analysis.

Figures 1.13 and 1.14 demonstrate the behaviour of log g derived from combined spectra. The combined fits of the artificial spectra suffer from a bias to higher surface gravities. When we combine the two spectra we are compensating for, or masking, the tail of low the log g values seen in fig. 1.12. It appears the mean log g value of the distribution moves towards higher values with decreasing signal-to-noise. In fig. 1.13 ($S/N = 100$) the mean is shifted $\sim +0.02$ dex while fig. 1.14 ($S/N = 50$) has been offset by $\sim +0.04$ dex. The gravities for cooler DB stars do not appear to suffer from this bias. The log g values presented in table 1.3 are uncorrected for this bias. We do not see any discrepancies in the simulations for derived effective temperatures.

We had persistent problems with the lowest quality spectra. The values from the blue spectra were significantly different than those of the combined fits. As discussed in sec.

1.4.1, these problems arise from flux normalization and the manner in which we connect the ends of the spectra. Table 1.4 shows a few different values we obtain by considering red and blue spectra independently. Various smoothing experiments with red spectra did not appreciably improve the quality of the fits. Four objects are treated separately: CBS 114, PG 1351+489, KUV05134+2605 and PG 1115+158. For these results, we were forced to rely only on the blue spectra for temperature and gravity. The red spectra were used only to derive the hydrogen abundance by enforcing the temperature and gravity found with the blue spectra upon the red. The other stars listed in the table were treated in the same manner as other higher S/N ratio spectra. The PG 1540+680 and PG 1456+103 objects display Balmer lines, which help to determine temperatures with less error. GD 233 is below 20,000K where we have less difficulty with the analysis. The agreement between red and blue parts for PG 1540+680 is marginal and eventually needs to be re-addressed along with the four stars considered separately. Unfortunately, we cannot reproduce this fitting method via Monte Carlo simulations so we do not include uncertainty estimates for these four stars. At worst, the temperature uncertainty will be similar to PG 1654+160, if we entirely ignore the information contained in the red spectra.

1.5.2 Spectra with two solutions

Several stars in table 1.3 have two solutions; two χ^2 minima exist based on the least-squares fitting technique. This situation is reminiscent of optical studies of ZZ Ceti stars (Daou et al. 1990). The solutions appear on either side of 22,000K. This is the temperature characteristic of the maximum strength (W_{max}) of He I lines (for our choice of convection) in pure helium atmospheres. Our non-linear fits give greater weight to the higher temperature solutions in all spectra. Results of the simulations have a certain number of artificial spectra choosing the lower temperature as the better fit, even though the artificial spectra were always created the using the hotter solution. The difference in χ^2 between the two solutions is small enough that random noise can cause hot spectra to be better described by the cooler solution. The

Atmospheric Parameters of DB Stars (ML2/α = 1.25)

Name	T_{eff}	$s(T_{eff})$	log g	s(log g)	log y	s(log y)	$>$ log y
LP 475-242	16200	$-360/+330$	8.71	$-0.05/+0.06$	4.4	$-0.11/+0.05$	
GD 378	16700	$-320/+280$	8.04	$-0.03/+0.04$	4.3	$-0.07/+0.12$	
PG 0129+246	16700	$-440/+590$	8.24	$-0.08/+0.07$	5.0	$-0.19/+0.27$	
GD 61	17600	$-290/+250$	8.14	$-0.05/+0.04$	3.9	$-0.08/+0.08$	
GD 243	18300	$-340/+430$	7.99	$-0.02/+0.06$	3.9	$-0.10/+0.15$	
Feige 4	18600	$-490/+190$	7.99	$-0.03/+0.05$	4.5	$-0.13/+0.14$	
GD 233	19200	$-1300/+1700$	8.04	$-0.06/+0.09$			4.9
GD 205	21000	$-1000/+1470$	8.06	$-0.04/+0.07$	3.7	$-0.27/+0.30$	
PG 1456+103	21400	$-840/+1300$	8.04	$-0.08/+0.09$	3.2	$-0.31/+0.30$	
PG 0921+091	21700	$-1100/+1700$	7.97	$-0.04/+0.06$	3.8	$-0.30/+0.28$	
GD 190	22000	$-2100/+1100$	7.94	$-0.02/+0.05$			4.8
GD 198	22000	$-2000/+1200$	7.87	$-0.01/+0.05$			4.7
PG 1540+680	22000	$-1200/+2700$	7.96	$-0.05/+0.08$	4.1	$-0.30/+0.59$	
PG 1115+158	22000		7.98		3.7		
KUV05134+2605	22500		8.14		3.2		
G 270-124	23300	$-940/+1200$	7.91	$-0.02/+0.05$	4.6	$-0.29/+0.21$	
	21500	$-590/+490$	7.91	$-0.02/+0.03$	4.7	$-0.27/+0.54$	
PG 1445+152	23400	$-1400/+1600$	7.86	$-0.00/+0.08$			4.6
	21000	$-1300/+1000$	7.84	$-0.04/+0.06$			4.8
PG 2234+064	23800	$-1300/+860$	8.00	$-0.01/+0.05$			4.7
	21500	$-1600/+470$	7.98	$-0.03/+0.04$			5.0
PG 2354+159	24000	$-1800/+1200$	8.02	$-0.01/+0.07$			4.5
	21500	$-1800/+400$	8.00	$-0.08/+0.04$			4.7
GD 358	24000	$-800/+940$	7.90	$-0.01/+0.05$			4.8
PG 2246+120	25900	$-1900/+2700$	7.90	$-0.01/+0.09$			4.3
PG 1351+489	26000		7.84				5.0
PG 1654+160	28000	$-4100/+960$	8.03	$-0.07/+0.00$			3.4
CBS 114	27200		8.00				3.9
EC20058-5234	28500	$-1900/+1700$	8.10	$-0.04/+0.03$			4.0
PG 0112+104	31000	$-700/+1300$	7.74	$-0.02/+0.05$			3.9

Table 1.3: Derived parameters for DB and DBA stars. The quoted errors are 68% confidence regions from simulations. Where no Hα is seen an upper limit of log y (y = N(He)/N(H)) is given. Cooler stars have smaller errors as expected from the sensitivity of equivalent widths to temperature. Comparison of uncertainties requires consideration of quality of the spectra. Stars with two sets of parameters are discussed in section 1.5.1.

Difficulties with low S/N spectra T_{eff};log g			
Name	*combined*	*blue*	*red*
PG 1115+158	22095; 8.00	22000; 7.97	25634; 8.39
KUV05134+2605	22000; 8.37	22783; 8.14	26950; 9.50
PG 1456+103	21395; 8.04	22548; 7.80	22968; 8.23
GD 233	19154; 8.04	18848; 8.00	18887; 7.82
CBS 114	23924; 8.06	27162; 8.00	28363; 8.42
PG 1540+680	22000; 7.96	22000; 7.93	23465; 8.58
PG 1351+489	25602; 8.00	26000; 7.84	30001; 8.45
LP475-242	16205; 8.71	16072; 8.68	16237; 8.03
G 270-124	23316; 7.91	24511; 7.94	20990; 7.68

Table 1.4: Selected results for the lowest S/N ratio red spectra. Signal-to-noise ratio increases from top to bottom. For CBS 114, the red and blue fits give similar T_{eff} values but there is difficulty in joining the spectra together. Other results show large variation in parameters due to poor flux normalization. In the case of G 270-124, the blue spectra suggests the hot solution, while the red spectra gives a better fit to the cool solution (see section 1.5.2). The final log g value is heavily weighted by the blue results, which are known to be biased (sec. 1.5.1). The anomalous gravity of LP 475-242, seen in the blue spectra does not appear to be caused by flux normalization.

proportion of simulations that find the lower solution is statistically significant for G 270-124 and PG 2234+064. In the case of PG 1445+152 the two solutions overlap. We refrain from assigning a higher confidence to either solution, as our analysis method may be biased towards the hot solution. For completeness, we have included both fits (figures 1.15, 1.16, 1.17& 1.18) in our list.

1.5.3 Simulation Results

DBA Simulations

In this section we present the results from the Monte-Carlo simulations. These figures are meant to highlight the temperature-hydrogen dependence for our solutions as well as provide the uncertainty estimates listed in table 1.3. We cannot simulate the method used to derive the hydrogen abundance (or upper limit) for the four stars we treated separately in table 1.4. We do not include errors for these objects.

A Monte Carlo run typically consisted of 1500 artificial spectra, each with random gaussian noise added. This number is sufficient to highlight the general outline of the solution space but

the volume is sparsely sampled for some of the results with large errors resulting in uneven contours. Fitted parameters from the artificial data sets were binned into a 20x20 grid in T_{eff} and log y. The number of fitted results in each bin were counted and normalized over the sum of all bins. This two-dimensional normalized grid is the probability distribution from which we estimate our confidence limits. The contours trace confidence regions from 10% to 100% in steps of 10%. In many of the stars, the orientation of the contours implies strong dependence between the parameters. If the parameters were independent then the confidence interval could be described by ellipses with semi-major axes parallel to a parameter axis.

Figures 1.19-1.28 show the behaviour of Monte-Carlo simulations for DBA stars. All graphs show a similar relation: higher hydrogen abundance results in increasing effective temperatures. This may seem to contradict the conclusions of B99. However, there is no ambiguity in the sub-type of these objects: all have prominent Hα lines. The locus of solutions can be thought of as a line tracing constant equivalent width of the Hα profile in the T_{eff}-log y plane. The contours are roughly elliptical with a semi-major axis that is at an angle to the parameter co-ordinate axis. This rotation of the contour's axis signifies dependence between T_{eff} and log y parameters.

The simulations of the cooler objects display a linear relation between T_{eff} and log y. We see a smaller slope for decreasing equivalent width of the Hα line. The stronger the Balmer line, the less uncertainty in the effective temperatures.

The DBA simulations above 20,000K have larger uncertainties towards higher T_{eff}. The slope of the linear relation turns over near this temperature and becomes horizontal. Near the maximum strength of neutral helium lines at 22,000K, the errors are dominated by theoretical and analysis difficulties (discussed in section 1.4.3).

Dual Solutions

Figures 1.29 - 1.32 demonstrate the parameter dependence for the stars we classified with two fits of comparable probability. The shape can be best described as an inverted 'V'; the vertex locates the maximum hydrogen content, near 22,000K. Tails extend to higher log y values for both higher and lower effective temperatures. The cooler side typically starts at a higher

log y value, which we expect as cooler stars are more sensitive to hydrogen. The reduced sensitivity of optical lines above 22,000K is seen by the larger contours for the hot solutions. In all four figures, there is a larger density of points around the hot solution. This behaviour is expected as all simulated spectra were created with the higher temperature solution.

DB Simulations

Figures 1.33 to 1.40 plot contours for stars where we do not detect Hα absorption. The three coolest objects in which we do not see Balmer lines have contours that are roughly symmetric along the vertical axis (figs. 1.33-1.35). Since the axis of the contours is roughly along a co-ordinate axis, we may consider our $T_{\rm eff}$ and log y estimates to be independent to first order. Variation of log y by 1 dex does not significantly change the mean effective temperature of these distributions. GD 190 and GD 198 both show a strong concentration of points at log y=5.0, this is an artifact of our interpolation scheme. Improvement of our interpolation scheme or a denser model grid could allow stricter log y limits, especially for GD 233.

The $T_{\rm eff}$-log y dependence seen for GD 358 and PG 1654+160 (figs. 1.36 & 1.37) is not apparent in the distributions of the cooler DB stars. This dependence is shown by the slope of the contours. This confirms the behaviour described in B99–namely spectroscopically invisible amounts of hydrogen can affect the derived effective temperature of the star.

Our simulations representing PG 1654+160 use only the blue spectra (Hβ) for fitting atmospheric parameters. It is worthwhile to compare the distribution of PG 1654+160 to GD 358. We see the difference in sensitivity to hydrogen by the slope of the contour bisectors between the two graphs. The contours of GD 358 cover 1 dex in log y and 2000K in $T_{\rm eff}$, while the larger contours of PG 1654+160 cover 2 dex in log y and 6000K in $T_{\rm eff}$. The steeper slope in the GD 358 distribution indicates that our log y upper limit constrains effective temperature to smaller uncertainty.

1.5.4 Detection Limits

In figure 1.41 we plot our abundances from table 1.3 and upper limits based on Monte Carlo simulations. Upper limits for non-detections of Hα show the maximum hydrogen abundance

and lowest T_{eff} consistent with the results in figs 1.33 - 1.40 (open circles). Further constraints on hydrogen would move these points down and to the left. We have plotted our estimated sensitivity limit for Hα. This limit is derived from simulations of red spectra and is meant to represent the performance we can expect from high S/N ($S/N = 100$) ratio optical spectroscopy. We have set the limit based on the central depth (4% of continuum flux) of the Hα profile.

Note that we cannot rule out the case of the hottest objects (PG 0112+104, EC 20058-5234, CBS 114) being white dwarfs with log y ratios near 4.0 (the typical ratio of most DBA stars). PG 1351+489 is placed well below our threshold with an upper limit of log $y \geq 5.0$. This star is one of our "difficult" spectra in table 1.4. Since we cannot simulate the method used to derive this limit, we place less confidence in this value. G 270-124 appears to have an error bar for log y extending below the sensitivity limit. This error covers both solutions in table 1.3 The upper limit of log $y \geq 5.2$ is appropriate for the lower effective temperature of 21,500K.

Currently only two objects have well determined log y limits near our detection threshold. The spectra of PG 0112+104 and GD 358 both have S/N ~100. Our current analysis method is more robust for the higher S/N ratio spectra; future refinements of our fitting techniques is unlikely to appreciably reduce their abundance limits. Our upper limits for PG 0112+104 and GD 358 are close to those in Provencal et al. (2000, hereafter PSTV00). We do not see any evidence of Balmer lines in PG 0112+104, although a N(He)/N(H) limit near their upper range of log $y = 4.0$ cannot be ruled out. Figure 1.42 shows our red spectra of PG 0112+104 assuming similar atmospheric parameters to PSTV00. We have used a lower surface gravity that is more consistent with our spectra.

The observed values of log y covers the range of 3.2-5.0 with an average of log y=4.0 in our sample of hot stars. This average agrees with that of SLG87. We conclude that most DBA stars have a canonical photospheric abundance of log y=4.0 over the temperature range of 22,000-14,000K. Considering the increase in our sensitivity to Balmer lines over this range, the increase by several orders of magnitude in the convection zone mass, and the range of white dwarf cooling age over these temperatures, this is an unexpected result and is a substantial

clue about the chemical evolution of DBA white dwarfs.

1.6 Discussion

1.6.1 DBA Fraction

The McCook and Sion catalog (McCook & Sion 1999) contains 151 unique entries of DB objects. After removal of mis-classified entries such as sdO stars (Bergeron et al. 2000) 81 have assigned temperature indexes. Of the 151 DB entries, 22 are sub-type DBA (or DBQA) for a DBA fraction of 15%.

How many of the DB stars listed have not been observed for trace photospheric hydrogen ? SLG87 found 16% (5/31 after removal of subdwarfs PG 1632+223 and PG 2234+034) of the stars in the Palomar-Green survey contained high Balmer lines. As the PG is a complete volume sample, there is probably an equivalent ratio among DB white dwarfs in general, thus the McCook & Sion catalog can be expected to contain a few unidentified DBA stars, most likely in the less studied southern hemisphere.

As discussed in Koester & Weidemann (1989), Balmer lines will be present to effective temperatures as low as 12,0000K in DB atmospheres. Below this temperature, the Lyman series of hydrogen lines in the UV are expected to be stronger. Thus, over the range of T_{eff} considered here and in SLG87, optical spectroscopy of Balmer lines will have comparable sensitivity to trace hydrogen as UV spectroscopy; Problems with geo-coronal emission creates its own set of analysis difficulties with Lyα profiles (Provencal et al. 2000).

DBA detections in SLG87 were based on the Balmer Hγ and Hβ lines. Our spectroscopy using Hα is more sensitive; we detect hydrogen at higher temperatures than could be studied by SLG87. Since we have spectra of all known DB2 stars, we can compare the DBA ratio as a function T_{eff} (SLG87 considered only DB3 PG objects). We have a 38% (7/18) ratio of DBA2 stars (figure 1.43), roughly double the fraction of DBA3 stars in SLG87. Our sensitivity for detecting Balmer lines is greater for cooler white dwarfs, thus we expect to find more DBA stars among the cooler DB3 objects. Solid observational evidence against this expected trend would indicate that DB2 stars intrinsically have more hydrogen in their photosphere or that

many DBA3 white dwarfs remain unidentified. Potentially the number of DBA3 stars could be doubled by a systematic survey for Hα over this temperature range if the fraction of DBA2 stars extends to cooler temperatures. Our sample in table 1.1 as a whole is 50% (13/26) composed of DBA stars. Several objects were known DBA sub-types beforehand and our survey is not complete in a statistical sense so this percentage is not representative of any sub-population of DB stars.

To enlarge our sample, we consider the nearly 80 DB white dwarf spectra we have obtained as part of our campaign to re-observe all bright northern non-DA stars. This sample is nearly complete for DB3 stars (and complete for DB2). Based on Hβ for stars not listed in this paper, roughly 30% of this sample are subtype DBA (figure 1.44).

The main conclusion of the DBA fraction of these different samples is that the canonical value of 20% of DB white dwarfs being DBA is probably an underestimate of the real number, based on our results for DB2 stars. Several authors have speculated that all DB stars contain trace hydrogen and thus the DBA fraction should continue to increase at all effective temperatures as observations improve. Trace hydrogen is most easily seen in cooler stars so in this scenario, we would expect more cool DBA stars to be found. The current observations suggest that this is not the case.

1.6.2 Theoretical equivalent widths

Equivalent widths of absorption lines are sensitive to the chosen convective efficiency of model atmospheres. This effect was investigated in Bergeron et al. (1995) for DA stars. Similar conclusions can be reached for DB stars: i) equivalent width is generally larger for higher values of log g, ii) the effective temperature at which the absorption lines reach their maximum strength (W_{max}) depends on the mixing length theory (MLT) used. iii) The equivalent width of absorption lines at all effective temperatures is somewhat dependent on the MLT.

Figures 1.45 and 1.46 plot theoretical equivalent widths (W_λ) as well as the measured values for our spectra. We have not estimated uncertainties for the measured values but they are expected to be proportional to the S/N of the spectra. We have chosen to display widths for the He I line λ7065Å as it is the most sensitive to effective temperature. There

is considerable spread in measured equivalent widths of the λ7065Å line. Equivalent widths are not consistent with theoretical values with the error bars for temperature. For this line, observational noise dominates over the small expected value of (W_λ) in this plot.

The λ4471Å profile has the largest equivalent width and thus will be the least affected by noise in the line wings. We can see that the largest widths, W_{max} does in fact occur near the temperature of 22,000K predicted by our current choice of MLT (ML2/α =1.25). Comparison of equivalent widths in this manner offers an independent method from Beauchamp (1995) to test ML2 as the best choice of MLT to describe DB atmospheres. There is still a large scatter in points above the theoretical values which may again be from noise. Several points are not consistent with the theoretical values within the T_{eff} error bars. In the case of gaussian-distributed measurement errors, we would expect an equal number of measurements to be above and below the expected value. Most points in the plot lie above the theoretical lines which may indicate a systematic effect in our analysis.

1.6.3 Temperature scale of pulsating DB white dwarfs

Adiabatic theory for white dwarf envelopes predicts that pulsation periods will be longer in cooler stars. The longest periods observed are those in the coolest pulsating stars. These periods are still less than predicted (Hansen et al. 1985; Kawaler et al. 1985) so another mechanism, such as convective mixing, is ultimately responsible for the cool boundary of the empirical instability strip. The increase in periods occurs because the lower envelope temperatures increases the thermal timescale of the mass above the driving region and from the convection zone which grows rapidly in depth as the pulsating star cools. The deepening convection zone is thought to carry the driving region deeper into the white dwarf envelope.

A temperature-period relation has been observed for DA pulsators (Winget & Fontaine 1982) and follows the behaviour predicted by theory. An earlier attempt with this kind of description for measured pulsation periods of DBV stars yielded inconsistent results (Koen et al. 1995). Although the boundaries for DBV temperatures have been known for some time (Liebert 1986; Thejll et al. 1991b), their relative surface temperatures within the instability strip remains uncertain. This work represents the continuation of efforts by B99 to define a

temperature scale for DBV white dwarfs based on optical spectroscopy.

Figure 1.47 shows our period-T_{eff} relationship. We see that there is general agreement with adiabatic theory: the shortest period star EC20058-5234(8) has the highest T_{eff} and the longest period variable PG 1115+158(3) occupies the low T_{eff} portion of the graph. As commented in Handler (2001) PG 2246+120(9) fills the gap in both temperature and period between the short period southern variable and "typical" DBV stars like PG 1351+489(4) and GD358(6).

We have chosen to use the dominant period, which is the period with the largest amplitude in a star's pulsation spectra, for our plots. We make the assumption that the dominant pulsation mode is a useful indicator of total driving power in DB stars (Bradley et al. 1993). Many DBV stars are multi-periodic and possibly have transient pulsation modes (Clemens et al. 1993), in addition limited time resolution means that amplitudes can be over-estimated from unresolved modes. Thus, the dominant period can change depending on which observations are used. The periods listed in table 1.1 are average values where multiple observations exist. For others, we have used published values. Future observing campaigns could remove this uncertainty in choice of dominant period and will most likely modify the behaviour of our graph.

More information can be obtained by graphing "weighted mean period" v/s temperature, which is a measure of the power pulsation in a white dwarf. Pulsation power is defined as the energy the driving region transfers to perturbations which cause the observed photosphere pulsations. Our weighted period is calculated by multiplying the dominant period listed in table 1.1 by the pulsation amplitude of that mode. This kind of figure will indicate effects such as saturation of the driving mechanism. In figure 1.48 we plot our version of the weighted period v/s effective temperature diagram. Assuming an inverse relation between power and temperature, this graph can be compared with Fig. 6b in Koen et al. (1995).

The mono-periodic DBV PG 1351+489(4) has the best determined period and pulsation amplitude (Kepler et al. 2000) of all variable DB stars; it is unlikely that its position as the largest weighted period will change. However, the summation over weighted periods in all identified modes, instead of one mode as we use here, would move objects such as well-

studied GD 358(6) (Vuille et al. 2000). From a theoretical viewpoint, it would be interesting to demonstrate that mono-periodic pulsating white dwarfs have more driving power than their multi-periodic cousins, particularly if future observations suggest that mono-periodicity is a transient state that all pulsating white dwarfs experience such as in the case of GD 358 (Nitta et al. 1999). There is significant scatter in this plot and large uncertainty in both temperature and period for several objects. The points do not follow the trend we expect from adiabatic theory. Beyond identifying the DB variable with the largest weighted period, current measurements are too uncertain to extract further information from this diagram.

1.6.4 DBV Instability Strip

B99 discussed the overall effect on the DB instability strip if all DB2 stars contained trace photospheric hydrogen. In this scenario, the instability strip would be compressed creating a "cold" strip that is ~2000K smaller than the "hot" case where (except for PG 1456+103) all DBV white dwarfs are described with helium photospheres. The actual results lie in between these scenarios. Our new temperatures indicate the stars marking the observed boundaries remain unchanged. The size of the instability strip has increased with our temperatures in table 1.3, as we have found PG 1456+103 to be cooler than B99. If we wish to consider temperatures in table 1 of B99, then PG 1115+158 will now denote the lower boundary of the instability strip, and the instability region now covers an interval larger than the "hot" case of ~6,600K.

Figure 1.49 shows our new instability strip. Despite an extensive literature search, there still remains a handful of objects that we do not know if they are photometric variables. The recent discovery of PG 2246+121 may indicate that some of these white dwarfs have never been monitored for variability. In addition to the objects in our graph, a few southern DB stars have temperatures possibly in the DB2 range (Wickramasinghe & Reid 1983).

In the case of DA stars, photometric or IUE observations have been used to choose between dual solutions derived from optical spectroscopy. For DB stars, errors associated with photometry and IUE spectra (Thejll et al. 1991a) are equal or greater than those in Table 1.3 and cannot be used to "break" the degeneracy of optical solutions. Pulsational instability

in DA white dwarfs is known to be related to the maximum strength of Balmer lines in DA stars. For the dual least-squares solutions DA stars known to be non-pulsators, Bergeron et al. (1995) chose the hotter solution. This choice is justified from evidence that all ZZ Ceti stars appear on the cooler side of W_{max} for Balmer lines. A similar argument can be applied for DB stars, although locations are reversed. We make the hypothesis that all DB variables exist at effective temperatures *greater* than that characteristic of W_{max} for He I lines. Therefore, we assume non-variable DB stars exist below W_{max}, the opposite side from the DA non-variables. Thus we would choose the cooler solutions for G 270-124, PG 1445+152 and PG 2354+159. No published observations are available to confirm whether PG 2234+064 is a non-pulsator.

It is worthwhile to mention that assuming the cooler temperatures for these dual-solution stars would result in an instability strip with only one known non-pulsating DBA object occupying the "pure helium" region of the instability strip. This object is LB 8827, a magnetic, strong-lined DBA star (Wesemael et al. 2001). We have used non-magnetic models to estimate T_{eff} which may result in a higher temperature than magnetic atmosphere models.

An empirical instability strip that does not include non-pulsators would have theoretical consequences. If we can confirm the DB instability strip contains only (non-magnetic) pulsating stars, this would suggest that instability to pulsations is a normal evolutionary phase for helium atmosphere white dwarfs. A similar scenario has been argued for DA variable stars.

Our results and those of B99 indicate that helium DB pulsators exist at temperatures above the characteristic T_{eff} for maximum strength of He I optical lines. The DBA variables appear to be exempt from this rule; they all appear at temperatures very close to W_{max} and possibly below. We cannot discern two characteristic χ^2 minima for these stars within the accuracy of our fitting methods. The precise temperature characteristic of W_{max} decreases slightly with increasing hydrogen content so it is no longer a fixed reference point for evaluating membership of pulsating DBA stars within the instability strip.

With our results, DBA variables white dwarfs are located in a region that contains several confirmed non-variable DB and DBA stars (Robinson & Winget 1983; Thejll et al. 1991b). Contrary to helium DB variables, co-location of pulsating and non-pulsating DBA white dwarfs suggests only a fraction of DBA stars experience instability to pulsations.

The location of the blue edge is sensitive to the assumed convection for pure helium atmosphere white dwarfs (Winget et al. 1983); however the red edge appears less sensitive. In the case of mixed H/He photospheres, convection is less important than pure helium atmosphere models. The temperatures of DBA stars, both variable and non-variable around the red edge have little dependence on the chosen MLT. Initial non-adiabatic helium models from BWW93 derive a theoretical red edge near 19,000K for standard ML2 convection. This is less than our empirical red edge of 24,000K for pure helium DBV objects. As expressed in BWW93, the most likely reason for the discrepancy between theory and observation is the lack of treatment of convective flux in pulsation models. Both theory (BWW93 show a variance of ~1500K of the red edge between ML2 and ML3 MLT) and observation (Beauchamp 1995 derives a difference of ~1800K between ML2 and ML3 helium atmosphere models near 22,000K) show the red edge to be only weakly dependent on MLT. For DBA models, this variation is even smaller. Any model that can explain the temperature difference of the empirical and theoretical red edge must account for other effects on the DBV pulsation structure; the difference cannot be explained by MLT alone.

The blue edge of the DBV instability strip can be determined from non-adiabatic theory. A recent investigation by Brassard & Fontaine (1997a,b) indicates a blue edge near 28,000K at log g=8.0 for ML2/α = 1.25 for helium evolutionary models. To our knowledge, no published models exist for pulsation instability in mixed H/He white dwarfs envelopes. Arguments based on thermal timescales and "poisoning" of the convection zone (Böhm-Vitense 1992) in a mixed envelope would derive a blue edge for DBA variables much cooler than this characteristic temperature. Our empirical instability strip stipulates that the DBA instability region could be a separate temperature range from a pure helium case.

1.6.5 Is hydrogen primordial or accreted?

What is the source of hydrogen in DB white dwarfs ? This has been an open question since the discovery of these stars. The two most probable sources are: i) hydrogen is left over from the post-AGB (pre-white dwarf) evolution as described in the float-up scenario (Liebert et al. 1987). AGB evolution theory yields an expected mass of $M_H = 10^{-4} M_\odot$ in white dwarfs

while the DBA phenomenon requires no more than $M_H = 10^{-13}M_\odot$. This difference has been unreconciled for several decades (D'Antona & Mazzitelli 1979) and is a major stumbling block in explaining DBA stars by normal stellar evolution. ii) The second choice is that all the hydrogen is removed from the envelope in the post-AGB phase and the hydrogen we see in non-DA stars has been accreted while they have been on the white dwarf cooling track.

If the bulk of photospheric hydrogen is accreted, the continued existence of several DB stars requires an explanation as to why these stars do not accumulate hydrogen while others do. Current evidence is not sufficient to resolve this issue. D'Antona & Mazzitelli (1979) were among the first to point out that the accretion rate needed to accumulate the hydrogen in DBA stars is below that of standard fluid accretion models (e.g. Bondi-Hoyle). More recently, the two-phase accretion model of Dupuis et al. (1993) offers a reasonably qualitative description for accretion of elements heavier than helium but still requires a hydrogen accretion rate $10^2 - 10^7$ times smaller than the rate for metals to match DBA observations.

Based on time-dependent diffusion calculations, Pelletier (1986) argued for accreted hydrogen. These results show that primordial hydrogen diluted throughout the DB helium convection zone would imply a lower limit of $\log y \gtrsim 7$, contrary to the of photospheric abundances of DBA stars of $\log y \sim 4$.

MacDonald & Vennes (1991, hereafter MV91) also favour accretion to explain the DBA abundance pattern. Their study used models with mixed H/He atmospheres in diffusive equilibrium. These calculations are noteworthy because they include the opacity effects of changing chemical abundances in the convection zone; to our knowledge this is the only publication to include this important effect first discussed in D'Antona & Mazzitelli (1979). They find a hydrogen mass of roughly $M_H = 10^{-15}M_\odot$ necessary to explain the DB gap. Similar reasoning to that of Dupuis et al. (1993) indicates DBA white dwarfs contain a factor of $10^2 - 10^3$ more hydrogen than expected via evolution with a constant primordial hydrogen mass. MV91 derive a lower limit of $M_H \gtrsim 10^{-16}M_\odot$ for the formation of an opaque H layer at the blue edge (~45,000K) of the DB gap. More recently, PSTV00 find very low hydrogen masses in a few DB stars for a variety of convection models. The mass limits in PSTV00 are much lower than those MV91 predict are needed to reproduce the DB gap.

Using similar assumptions to PSTV00, we deduce hydrogen masses for objects in our sample. We have used the latest envelope models of Fontaine et al. (2001) to establish convection zone mass. We assume that a fixed amount of hydrogen is uniformly mixed throughout the convection zone and only the deepening convective zone will cause changes in the observed N(He)/N(H) ratio [1]. We assume a "pure dilution" scenario where the addition of hydrogen has negligible impact on the structure and evolution of the otherwise pure helium atmosphere.

For the moment, we have used envelope parameters more appropriate for DA white dwarfs. We have chosen a pure helium "thick" envelope ($10^{-2}M_{\odot}$) with ML2/α =0.6 MLT. At temperatures above roughly 20,000K the mixing length has little effect on the convective mass. The helium convection zone is always several orders of magnitude smaller than the envelope mass; thus "thick" versus "thin" envelopes have no impact on photospheric abundances.

To extend our baseline to lower temperatures, we have included all DBA spectra in our database of 80 DB stars (fig. 1.44). Many of these were presented in Beauchamp (1995), however we include several newly discovered DBA stars from unpublished blue spectra acquired in 1995. The results of Beauchamp (1995) (excluding stars we have re-analyzed including new red spectra) use the older fitting code from HWSBB01. At the temperature range below 18,000K there could be as much as a 5% discrepancy in $T_{\rm eff}$ between our two fitting techniques. In addition, the assumed convective efficiency is different for the synthetic spectra and the envelope models of Fontaine et al. (2001). However, choice of convection is less important in cooler atmospheres as the temperature gradient is nearly adiabatic. The values presented here should be considered preliminary, they are meant to outline the general behaviour of hydrogen mass for varying effective temperatures. This combined sample contains nearly 30 DBA stars with accompanying CCD spectroscopy. This is the largest sample of DBA white dwarfs studied to date.

Figure 1.50 plots our derived DBA abundances and temperatures, as well as upper limits for hydrogen non-detections from figure 1.41. The gap near 20,000K is probably an artificial bias of our fitting code. As mentioned in section 1.4.2, our new lest-squares fitting code has a

[1] It is worthwhile to note this procedure causes a discontinuous abundance gradient at the bottom of the convection zone. Pelletier (1986) has shown that as much as 80% of the hydrogen will thus be moved below the convection zone by normal diffusion.

tendency to find a T_{eff} of 22,000K for blue spectra with temperatures in the range of 22,000-20,000K. Below 19,000K DBA stars have an average abundance of log y=4.5 which is slightly below the average abundances in PSTV00 and Dupuis et al. (1993). This most likely results from our new DBA spectra with log y ~5.0. In cool DBA stars, log y values of 5.0 are now detected from our CCD spectra.

We also note that three hot DBA stars have hydrogen abundance ratios an order of magnitude greater than all other DBA white dwarfs. Two of these object are the magnetic, spectroscopic-variable white dwarfs LB 8827 (Wesemael et al. 2001) and Feige 7 (Achilleos et al. 1992). The third object is the relatively unknown star LP 497-114, a DBA white dwarf with a strong Hβ line. This star has been previously classified as a DA4 from IUE observations (Kepler & Nelan 1993). From its location in our plot near the magnetic stars, LP 497-114 merits further observations.

We have also plotted the models from MV91 that use their 'S1' (Schwarzschild criterion for convection with a mixing length ratio of one) envelope models. This mixing length prescription is different from the Böhm-Vitense MLT we use for our ML2 models. MV91 describe their convection zones as similar to the ML2 models of Fontaine et al. (1987). For this preliminary investigation, we feel they are sufficient to demonstrate the major differences with the current Fontaine et al. (2001) envelopes.

In fig. 1.50 we have shown the ML2 model assuming $M_H = 10^{-18} M_\odot$ of hydrogen. We have chosen this mass for two reasons: first it approximately matches the upper limits we derive for the hottest DB stars; second, we feel that this is a sufficiently small quantity of hydrogen as to not affect the development of the helium envelope structure. In other words, we believe this is the *largest* quantity of H one can safely mix in a helium convection zone without significantly changing the opacity of the atmosphere layers. This is a critical assumption that nearly every previous study (Pelletier 1986; Shipman et al. 1987; Dupuis et al. 1993; Provencal et al. 2000) has made using larger hydrogen masses.

The consequences of assuming "pure dilution" are clearly seen by comparing the ML2 model ($10^{-18} M_\odot$ of hydrogen) and the S1 model with $M_H = 10^{-16} M_\odot$. At T_{eff} ~19,000K the photospheric H/He ratio differs by nearly four orders of magnitude (and six orders of

magnitude by 15,000K) even though the hydrogen mass differ by only two decades. The cause is "poisoning" of the convection zone from the changing chemical abundance as we previously eluded. This effect is not considered in our ML2 model. The difference between observed log y and the theoretical "un-poisoned" abundance ratios is what has led previous authors to conclude that accretion of interstellar hydrogen is necessary to explain the DBA phenomenon. Even accounting for opacity changes, MV91 concluded that cool DBA stars contain $M_H = 10^{-13}M_\odot$, a mass too large to explain the red edge of the DB gap by convective mixing. Our new DBA2 observations require smaller masses of approximately $M_H = 10^{-16}M_\odot$ for the MV91 models to match the observed abundance pattern. This mass is within the mass range needed by the float-up model of Liebert et al. (1987).

We also note that the range of hydrogen masses of $10^{-16} - 10^{-13}M_\odot$ give generally the same log y ratio at 16,000K for the S1 models. At this temperature the helium convection zone has been "saturated" by the more opaque hydrogen and the observed log y ratio is less sensitive to details of hydrogen masses in the envelope. The exact log y value these "saturated" envelopes exhibit is likely to be model dependent.

Time-dependent accretion calculations in Dupuis et al. (1993) predict that hydrogen abundances will increase as the surface temperature decreases. Our results in fig. 1.50 suggest the abundance ratio is roughly constant. If hydrogen in DBA3 stars has been accreted, we estimate an upper limit for continuous accretion of $\dot{M} = 10^{-21}M_\odot/yr$ of solar composition material is needed to reproduce the observed abundances. To derive this estimate, we assume that a DB star has $M_H = 10^{-18}M_\odot$ at the red edge of the DB gap (30,000K) and accretion of hydrogen is "turned on" at a temperature of 22,000K.

The accretion hypothesis still does not offer an explanation as to why some DB stars in our sample do not show any evidence of hydrogen in their spectra. Given the white dwarf age of cooler stars such as GD 233 (~100Myr), it is likely they have encountered hydrogen in the ISM during its orbit. The accretion scenario may explain the global abundances of DBA stars but it is difficult to reconcile with individual objects like GD 233.

Like previous authors, if we assume hydrogen is accreted then we must invoke a screening processes to explain the low hydrogen masses for DBA stars. We have constrained accretion to

a sufficiently small rate that essentially only hydrogen atoms trapped within the gravitational well of a DB white dwarf will remain (i.e. the Eddington limit, D'Antona & Mazzitelli (1979)).

Given our preliminary conclusions and the variation in analysis methods used between theoretical and observed values, we are unable to estimate hydrogen masses of individual DBA stars with confidence. Further study with consistent convective models is highly desirable. We can at least make two important conclusions from our results: i) at least two DB stars: PG 0112+104 and GD 358 have hydrogen masses of $M_H \lesssim 10^{-18} M_\odot$. This low hydrogen content implies these stars would have never formed an opaque hydrogen layer over the temperature interval of the DB gap, nor would they have formed a visible stratified layer of hydrogen such as believed for the DAB star GD323 (Koester 1991). ii) Pure helium envelope structures are not valid for studying DBA stars. In particular, changing chemical abundances of cooling mixed atmospheres must be explicitly addressed when modeling convection zones.

1.7 Summary

We have combined new red spectra (λ5700-λ7100) with previous blue spectra (λ3700-λ5100) to determine the effect of hydrogen on the effective temperatures of hot DB white dwarfs. The new spectra, which are centered on the Balmer Hα line, afford a higher sensitivity to small quantities of hydrogen in the helium dominated atmospheres. New mixed H/He atmosphere models including Hα and He I lines at red optical wavelengths, allow us to derive a limit of log $y \gtrsim 4.0$ for the hottest DB object, PG 0112+104. We also find log $y \gtrsim 4.8$ for the pulsating DB star GD 358. These limits are in close agreement with the results of PSTV00 based on Lyα UV spectroscopy.

Our study comprised all spectroscopically identified hot DB2 white dwarfs. Of these 22 stars, 10 are subtype DBA with a typical photospheric abundance of log $y \sim 4.0$. A few stars in our sample have no published null results for photometric variability. At least two of the DBA2 stars are magnetic and spectroscopically variable. We find the DBA LP 497-114 has a hydrogen abundance and temperature similar to these magnetic white dwarfs. We estimate an upper limit of log $y \gtrsim 4.0$ for hot DB stars where we do not see Balmer lines (with the exception of PG 1654+160 with log $y \gtrsim 3.4$).

Our new temperatures imply an empirical instability strip extending from roughly 28,000K to 21,000K. We find the coolest variable DB stars contain trace amounts of hydrogen. The helium DBV stars cover a temperature range of 28,000K-24,000K, while the DBAV objects occupy a narrow range between 22,500-21,000K. Further theoretical work is needed to test if the blue edge of DBA white dwarfs is much cooler than the corresponding boundary for the helium DB stars.

We have used Monte Carlo simulations to test the reliability of our results. We find hotter stars have larger uncertainties, as expected from the decreased sensitivity of optical helium lines at higher temperatures. We also see that our estimated errors are dependent on the S/N of the spectra and the strength of the Hα profile. Comparison with results based only upon blue spectra indicate our new surface gravities are systematically different with our new analysis methods. Our current non-linear fitting technique has considerable difficulty when He I lines are near their maximum width encompassing temperatures over the range of 21,000 to 24,000K.

We derive hydrogen masses using ML2 MLT. We find results similar to PSTV00; at least four of the hottest DB stars have hydrogen masses too small to have ever appeared as DA white dwarfs at temperatures characteristic of the DB gap. We compare current helium envelope models using ML2 mixing length with older mixed hydrogen/helium envelope models that specifically account for the opacity of hydrogen. The hydrogen opacity can have a significant role on the development of the helium convection zone. We conclude that neither model can fully explain the observed abundance pattern of DBA stars, although the models of MV91 provide a closer match to DBA observations.

To explain the photospheric H/He ratios seen in DBA white dwarfs, we must assume that these stars are accreting hydrogen from the ISM. We estimate an accretion rate of $\dot{M}_H = 10^{-21} M_\odot/\mathrm{yr}$ is necessary to describe simultaneously the hydrogen masses in DBA2 and DBA3 stars. This accretion rate is much lower than that found by previous studies.

References

Aannestad, P. A. & Sion, E. M. 1985, AJ, 90, 1832

Achilleos, N., Wickramasinghe, D. T., Liebert, J., Saffer, R. A., & Grauer, A. D. 1992, ApJ, 396, 273

Beauchamp, A. 1995, PhD thesis, Université de Montréal

Beauchamp, A., Wesemael, F., & Bergeron, P. 1997, ApJS, 108, 559

Beauchamp, A., Wesemael, F., Bergeron, P., Fontaine, G., Saffer, R. A., Liebert, J., & Brassard, P. 1999, ApJ, 516, 887, (B99)

Beauchamp, A., Wesemael, F., Bergeron, P., & Liebert, J. 1995a, ApJ, 441, L85

Beauchamp, A., Wesemael, F., Bergeron, P., Liebert, J., & Saffer, R. A. 1996, in ASP Conf. Ser. 96: Hydrogen Deficient Stars, 295

Beauchamp, A., Wesemael, F., Bergeron, P., Saffer, R. A., & Liebert, J. 1995b, in LNP Vol. 443: White Dwarfs, 108

Bergeron, P., Saffer, R. A., & Liebert, J. 1992, ApJ, 394, 228, (BSL92)

Bergeron, P., Wesemael, F., Lamontagne, R., Fontaine, G., Saffer, R. A., & Allard, N. F. 1995, ApJ, 449, 258

Bergeron, P., Wesemael, F., & Saffer, R. A. 2000, PASP, 112, 837

Böhm-Vitense, E. 1992, Stellar Astrophysics: Stellar Structure and Evolution, Vol. 3 (Cambridge University Press)

Bradley, P. A., Winget, D. E., & Wood, M. A. 1993, ApJ, 406, 661, (BWW93)

Brassard, P. & Fontaine, G. 1997a, in ASSL Vol. 214: White dwarfs, 451

Brassard, P. & Fontaine, G. 1997b, in The Third Conference on Faint Blue Stars, 485

Clemens, J. C., Barstow, M. A., Nather, R. E., Winget, D. E., Bradley, P. A., Claver, C. F., Dixon, J. S., Kanaan, A., Kleinman, S. J., Provencal, J., Wood, M. A., Sullivan, D., Wickramasinghe, D. T., Ferrario, L., Marar, T. M. K., Seetha, S., Ashoka, B. N., Leibowitz, E., Mendelson, H., O'Donoghue, D., Buckley, D. A., Chen, A.-L., Zola, S., Krzesinski, J., Moskalik, P., Vauclair, G., Fremy, J.-R., Chevreton, M., Kepler, S. O., & Odilon, G. 1993, in NATO ASIC Proc. 403: White Dwarfs: Advances in Observation and Theory, 515+

D'Antona, F. & Mazzitelli, I. 1979, A&A, 74, 161

Daou, D., Wesemael, F., Fontaine, G., Bergeron, P., & Holberg, J. B. 1990, ApJ, 364, 242

Dappen, W., Anderson, L., & Mihalas, D. 1987, ApJ, 319, 195

Dupuis, J., Fontaine, G., & Wesemael, F. 1993, ApJS, 87, 345

Dupuis, J., Pelletier, C., Fontaine, G., & Wesemael, F. 1987, in IAU Colloq. 95: Second Conference on Faint Blue Stars, 657

Eggen, O. J. & Greenstein, J. L. 1965, ApJ, 141, 83

Fontaine, G., Brassard, P., & Bergeron, P. 2001, PASP, 113, 409

Fontaine, G., Tassoul, M., & Wesemael, F. 1987, in IAU Colloquium No 95., The Second Conference on Faint Blue stars, 657

Green, R. F., Schmidt, M., & Liebert, J. 1986, ApJS, 61, 305

Handler, G. 2001, MNRAS, 323, L43

Hansen, B. M. S. 1999, ApJ, 520, 680

Hansen, C. J., Winget, D. E., & Kawaler, S. D. 1985, ApJ, 297, 544

Hummer, D. G. & Mihalas, D. 1988, ApJ, 331, 794

Hunter, C., Wesemael, F., Saffer, R. A., Bergeron, P., & Beauchamp, A. 2001, in 12th European Workshop on White Dwarfs, in press (HWSBB01)

Kawaler, S. D., Winget, D. E., & Hansen, C. J. 1985, ApJ, 298, 752

Kepler, S. O. & Nelan, E. P. 1993, AJ, 105, 608

Kepler, S. O., Robinson, E. L., Koester, D., Clemens, J. C., Nather, R. E., & Jiang, X. J. 2000, ApJ, 539, 379

Koen, C., O'Donoghue, D., Stobie, R. S., Kilkenny, D., & Ashley, R. 1995, MNRAS, 277, 913

Koester, D. 1991, in NATO ASIC Proc. 336: White Dwarfs, 343

Koester, D. & Weidemann, V. 1989, A&A, 219, 276

Koester, D. & Wolff, B. 2000, A&A, 357, 587

Liebert, J. 1986, in ASSL Vol. 128: IAU Colloq. 87: Hydrogen Deficient Stars and Related Objects, 367

Liebert, J., Fontaine, G., & Wesemael, F. 1987, Memorie della Societa Astronomica Italiana, 58, 17

MacDonald, J. & Vennes, S. 1991, ApJ, 371, 719, (MV91)

McCook, G. P. & Sion, E. M. 1999, ApJS, 121, 1

Metcalfe, T. S., Nather, R. E., & Winget, D. E. 2000, ApJ, 545, 974

Michaud, G., Fontaine, G., & Charland, Y. 1984, ApJ, 280, 247

Napiwotzki, R. 1999, A&A, 350, 101

Nitta, A., Winget, D. E., Kepler, S. O., & et al. 1999, in ASP Conf. Ser. 169: 11th European Workshop on White Dwarfs, 104

Pelletier, C. 1986, PhD thesis, Université de Montréal

Pelletier, C., Fontaine, G., & Wesemael, F. 1989, in IAU Colloq. 114: White Dwarfs, 249

Press, W., Flannery, B., Teukolsky, S., & Vetterling, W. 1989, Numerical Recipes, 2nd edn. (Cambridge Univ. Press)

Provencal, J. L., Shipman, H. L., Thejll, P., & Vennes, S. . 2000, ApJ, 542, 1041, (PSTV00)

Robinson, E. L. & Winget, D. E. 1983, PASP, 95, 386

Saffer, R. A., Liebert, J., & Olszewski, E. W. 1988, ApJ, 334, 947

Shipman, H. L., Liebert, J., & Green, R. F. 1987, ApJ, 315, 239, (SLG87)

Sion, E. M. 1984, ApJ, 282, 612

Sion, E. M., Greenstein, J. L., Landstreet, J. D., Liebert, J., Shipman, H. L., & Wegner, G. A. 1983, ApJ, 269, 253

Thejll, P., Vennes, S., & Shipman, H. L. 1991a, ApJ, 370, 355

Thejll, P., Vennes, S., & Shipman, H. L. 1991b, in NATO ASIC Proc. 336: White Dwarfs, 257

Vuille, F., O'Donoghue, D., Buckley, D. A. H., Massacand, C.-M., Solheim, J. E., Bard, S., Vauclair, G., Giovannini, O., Kepler, S. O., Kanaan, A., Provencal, J. L., Wood, M. A., Clemens, J. C., Kleinman, S. J., O'Brien, M. S., Nather, R. E., Winget, D. E., Nitta, A., Klumpe, E. W., Montgomery, M. H., Watson, T. K., Bradley, P. A., Sullivan, D. J., Wu, K., Marar, T. M. K., Seetha, S., Ashoka, B. N., Mahra, H. S., Bhat, B. C., Babu, V. C., Leibowitz, E. M., Hemar, S., Ibbetson, P., Mashals, E., Meištas, E., Moskalik, P., Zoła, S., Krzesiński, J., & Pajdosz, G. 2000, MNRAS, 314, 689

Wesemael, F. 1979, A&A, 72, 104

Wesemael, F., Green, R. F., & Liebert, J. 1985, ApJS, 58, 379

Wesemael, F., Liebert, J., Schmidt, G. D., Beauchamp, A., Bergeron, P., & Fontaine, G. 2001, ApJ, 554, 1118

Wesemael, F. & Truran, J. W. 1982, ApJ, 260, 807

Wickramasinghe, D. T., Hintzen, P., Strittmatter, P. A., & Burbidge, E. M. 1975, ApJ, 202, 191

Wickramasinghe, D. T. & Reid, N. 1983, MNRAS, 203, 887

Wickramasinghe, D. T. & Whelan, J. A. J. 1977, MNRAS, 178, 11

Winget, D. & Fontaine, G. 1982, in Pulsations in Classical and Cataclysmic Variable Stars, ed. J. Cox & C. Hansen (University of Colorado, Boulder), 46

Winget, D. E., van Horn, H. M., Tassoul, M., Hansen, C. J., & Fontaine, G. 1983, ApJ, 268, L33

1.9 Figures

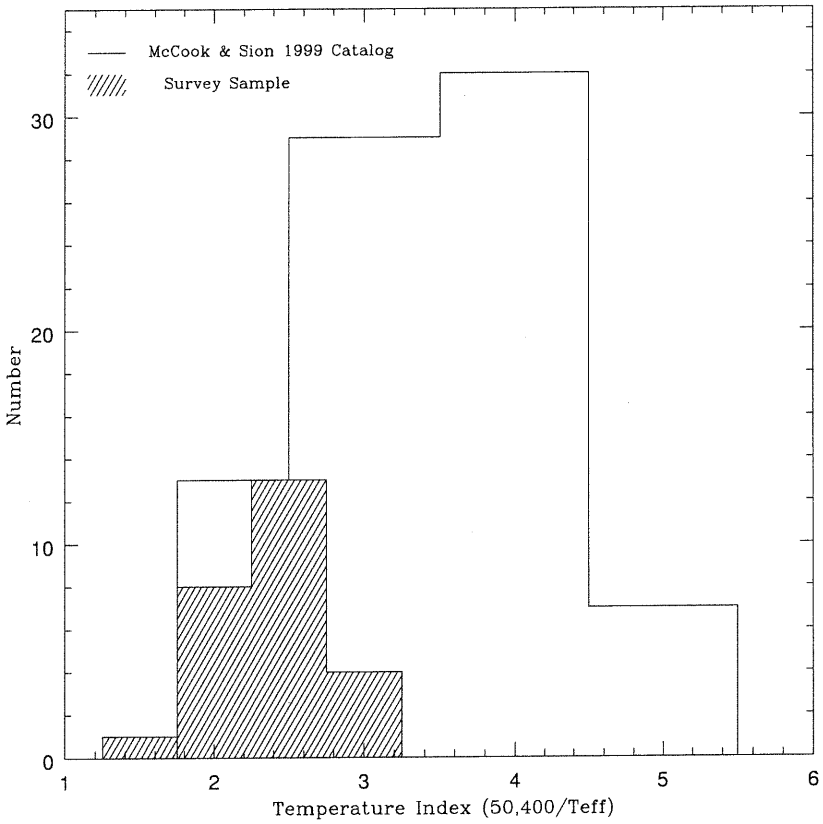

Figure 1.1: Comparison of survey sample with DB stars in McCook & Sion Catalog. We have used the temperatures in Table 1.3 for our sample and half-integer bins. The catalog sample uses whole integer bins. With the inclusion of hydrogen, a few stars have been shifted from the DB2.5 to the DB3.0 bin in our results. We have classified PG 0112+104 as DB1.5.

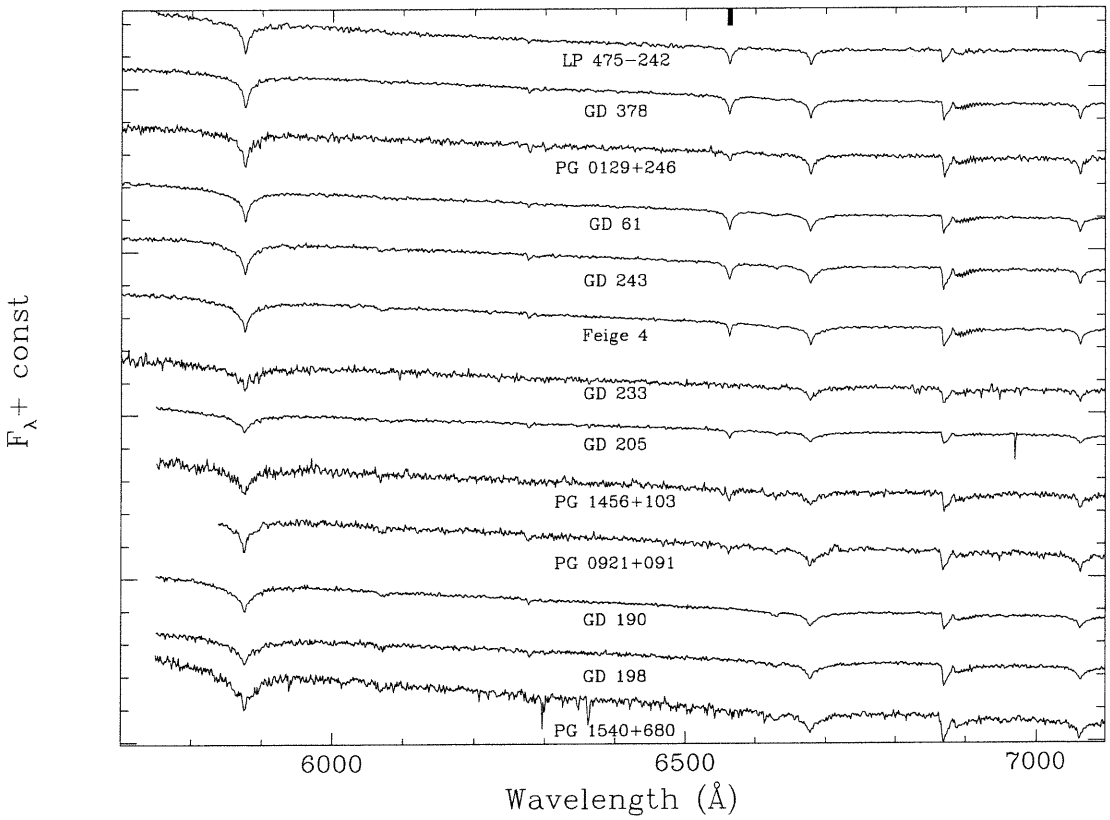

Figure 1.2: New spectra covering λ5700-7100 Å. The cool DBA stars in our sample all show strong Hα . Only GD 190, GD 198 & GD 233 do not show Balmer lines in the cooler half of our sample. Features near λ6900Å and λ6300Å are terrestrial absorption bands. Location of Hα is shown by the tickmark at the top of the graph.

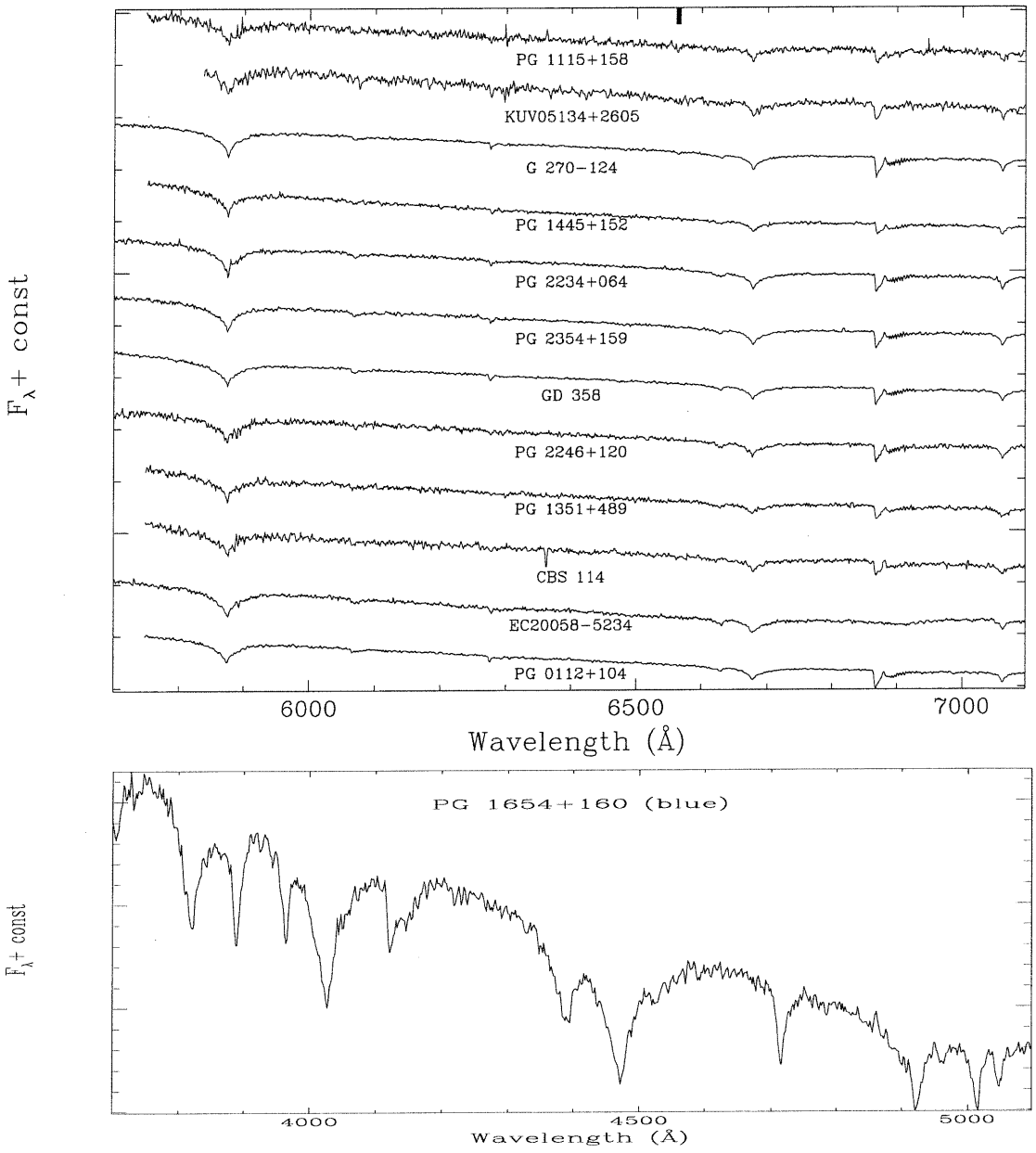

Figure 1.3: fig. a: New spectra covering $\lambda 5700 - 7100$ Å. Only three stars: G 270-124, KUV05134+2605 & PG 1115+158 show a Hα profile. EC20058-5234 exhibits unusual line fluxes near $\lambda 7000$ Å. Features near $\lambda 6900$Å and $\lambda 6300$ Å are terrestrial absorption bands. Location of Hα is shown by the tickmark at the top of the graph. fig. b: Blue spectra for PG 1654+160 which covers $\lambda 3700 - 5100$ Å.

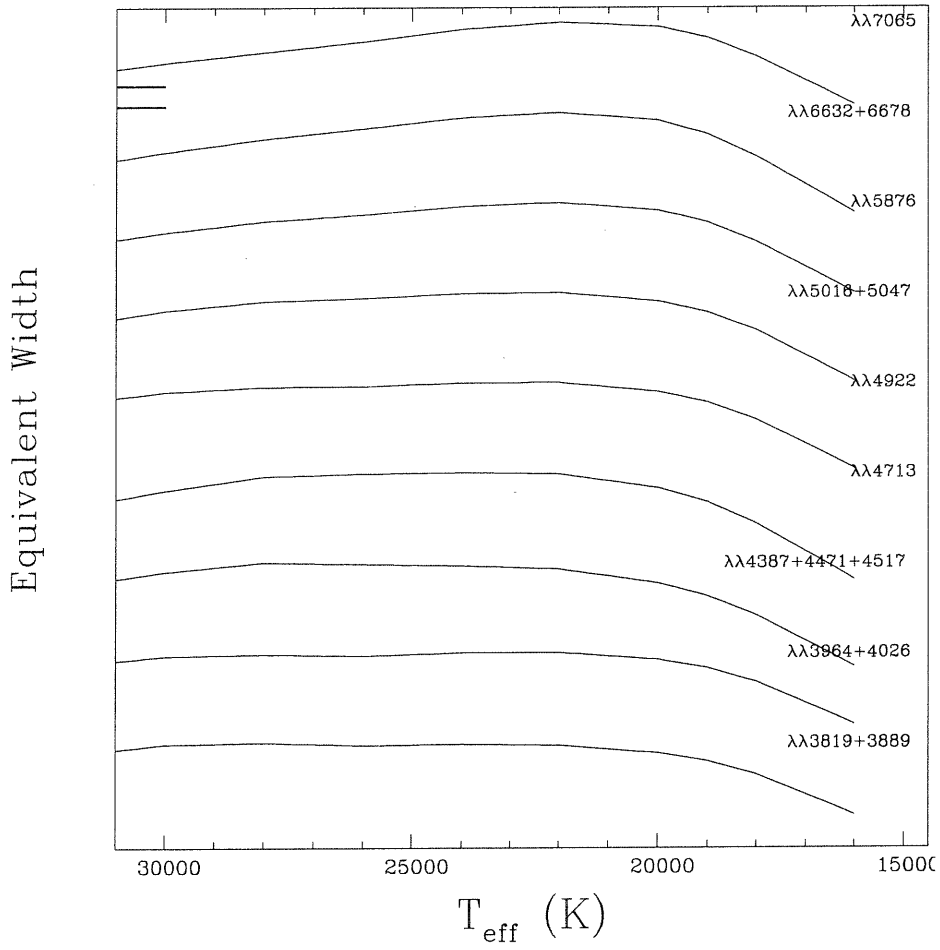

Figure 1.4: Equivalent widths of lines or groups of overlapping lines for DB atmospheres with negligible hydrogen content. Each width has been normalized to its maximum value (near 22,000K). Tickmarks indicate a 10% change in equivalent width. Note that the slope above 22,000K becomes more pronounced for longer wavelengths.

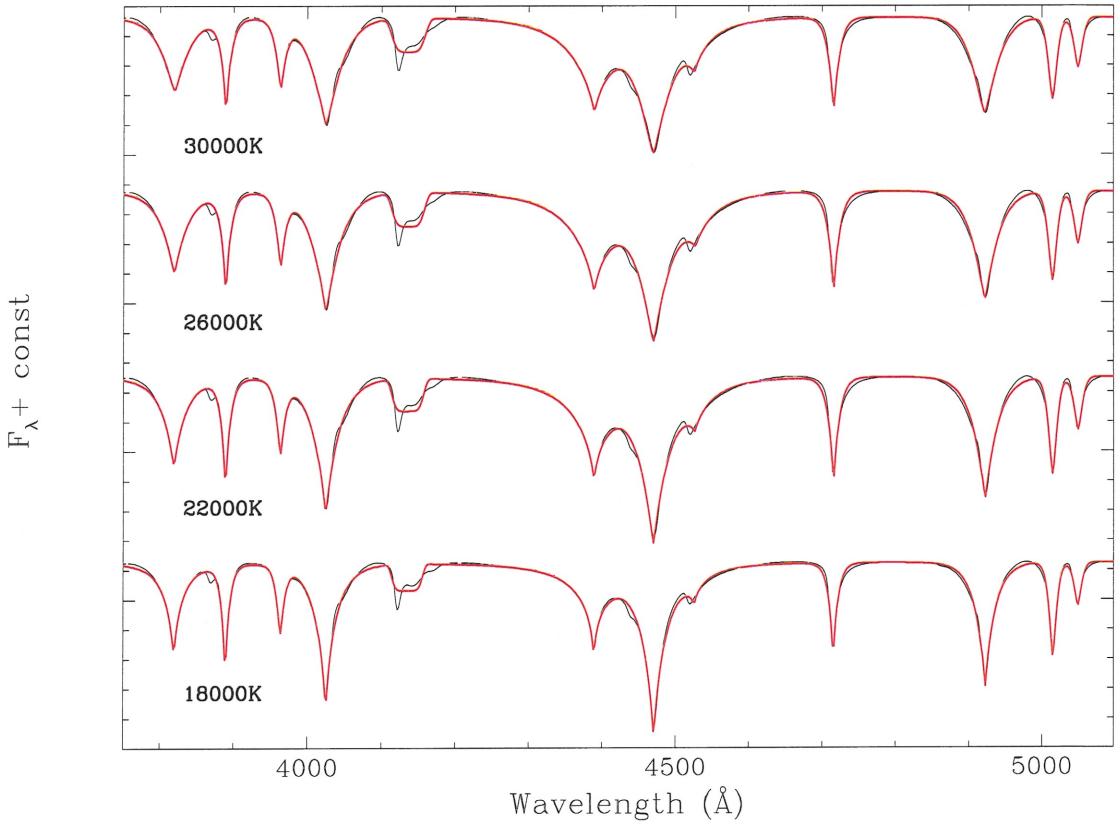

Figure 1.5: Examples of fits of pseudo-gaussian profiles to normalized model (i.e. noiseless) spectra. Models are black lines and pseudo-gaussians are red. Pseudo-gaussians are unable to reproduce the He I lines in detail. Much of the problem can be attributed to the asymmetry of synthetic spectra.

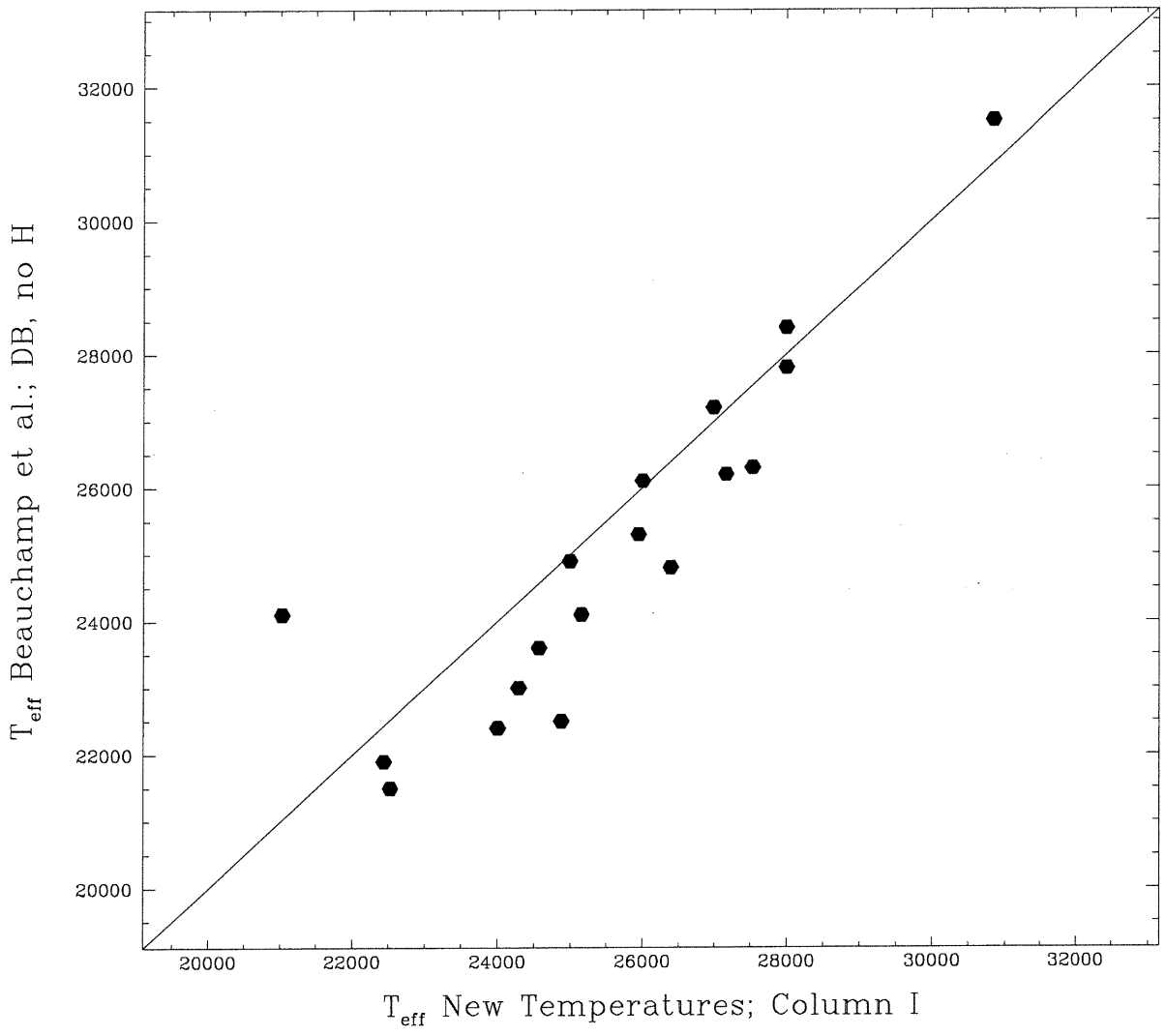

Figure 1.6: Comparison of temperatures from first column of Table 1 in Beauchamp et al. (1999) with values from our new analysis using only blue spectra derived in a similar manner as B99. The models in B99 use pure He atmospheres while we use mixed H/He atmospheres for our new temperatures. We choose the lowest hydrogen abundance (N(He)/N(H)=$10^{5.5}$) in our model grid, which is below the detection limit of Hβ for the temperature range in this figure. We generally derive higher effective temperatures with our new fitting code. Note that we find a much lower temperature for GD 205 (point furthest left) than B99.

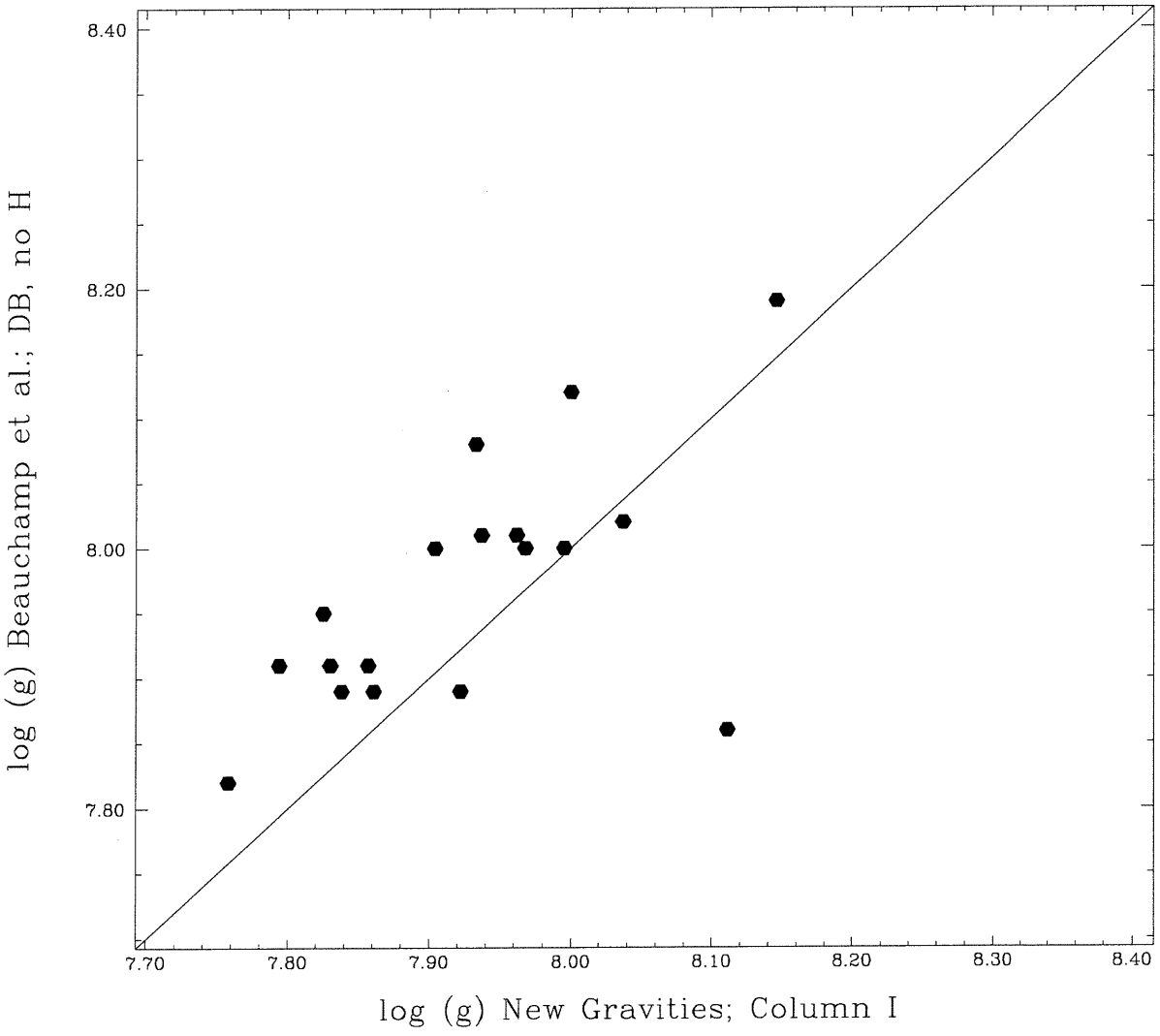

Figure 1.7: Comparison of surface gravities from first column of Table 1 in Beauchamp et al. (1999) with values derived from our new analysis using only blue spectra. Our new least-squares fits find systematically lower log g values, with the exception of EC20058-5234 at $(8.10, 7.85)$.

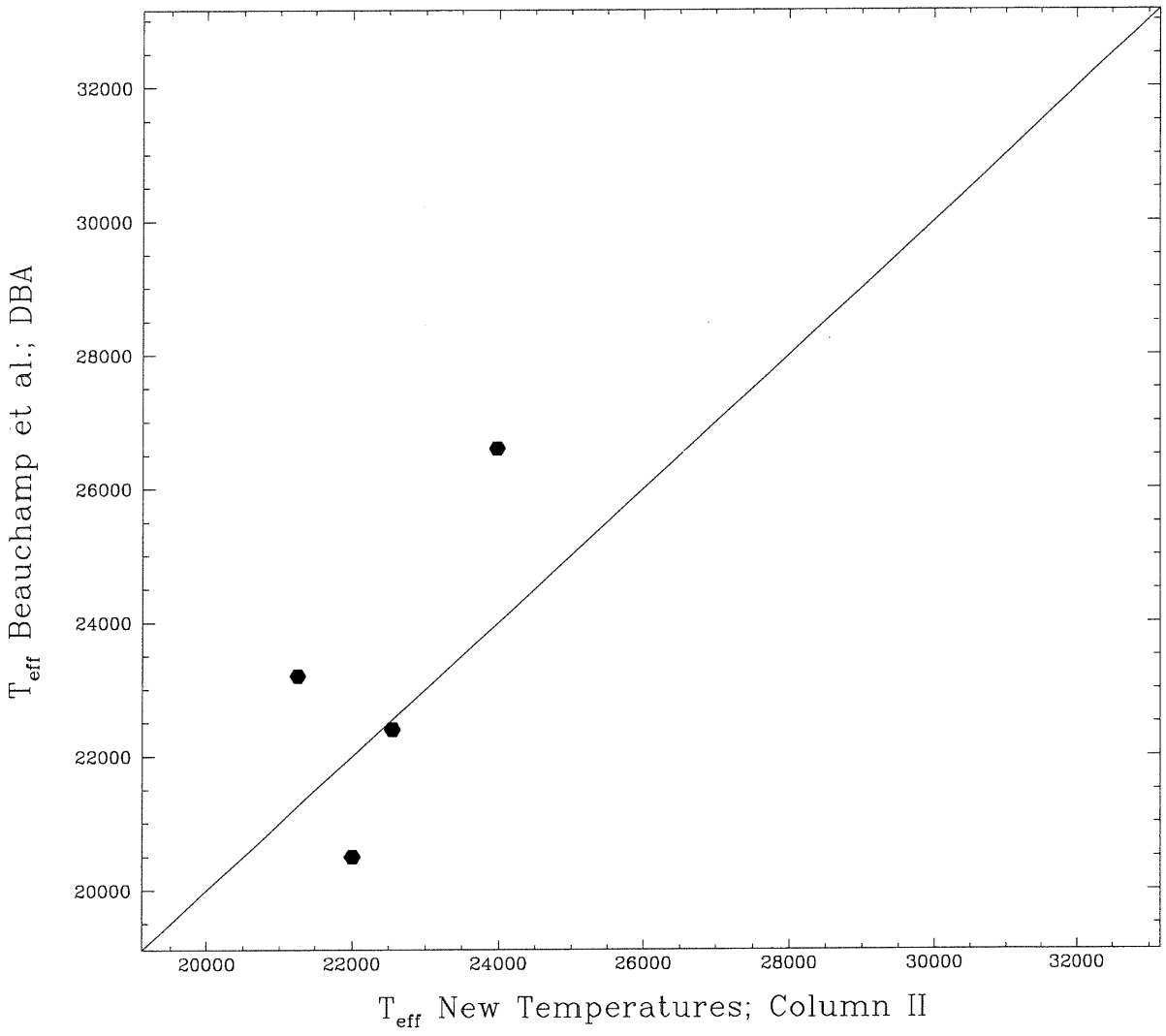

Figure 1.8: Comparison of temperatures from DBA column of Table 1 in Beauchamp et al. (1999) with values from our new analysis using only blue spectra. These stars all show prominent Hβ lines. As hydrogen content was a free parameter in these fits, the variation of T_{eff} follows from the change in the N(He)/N(H) ratio. PG 1149-133 & PG 1326-037 are overlapping points on this diagram.

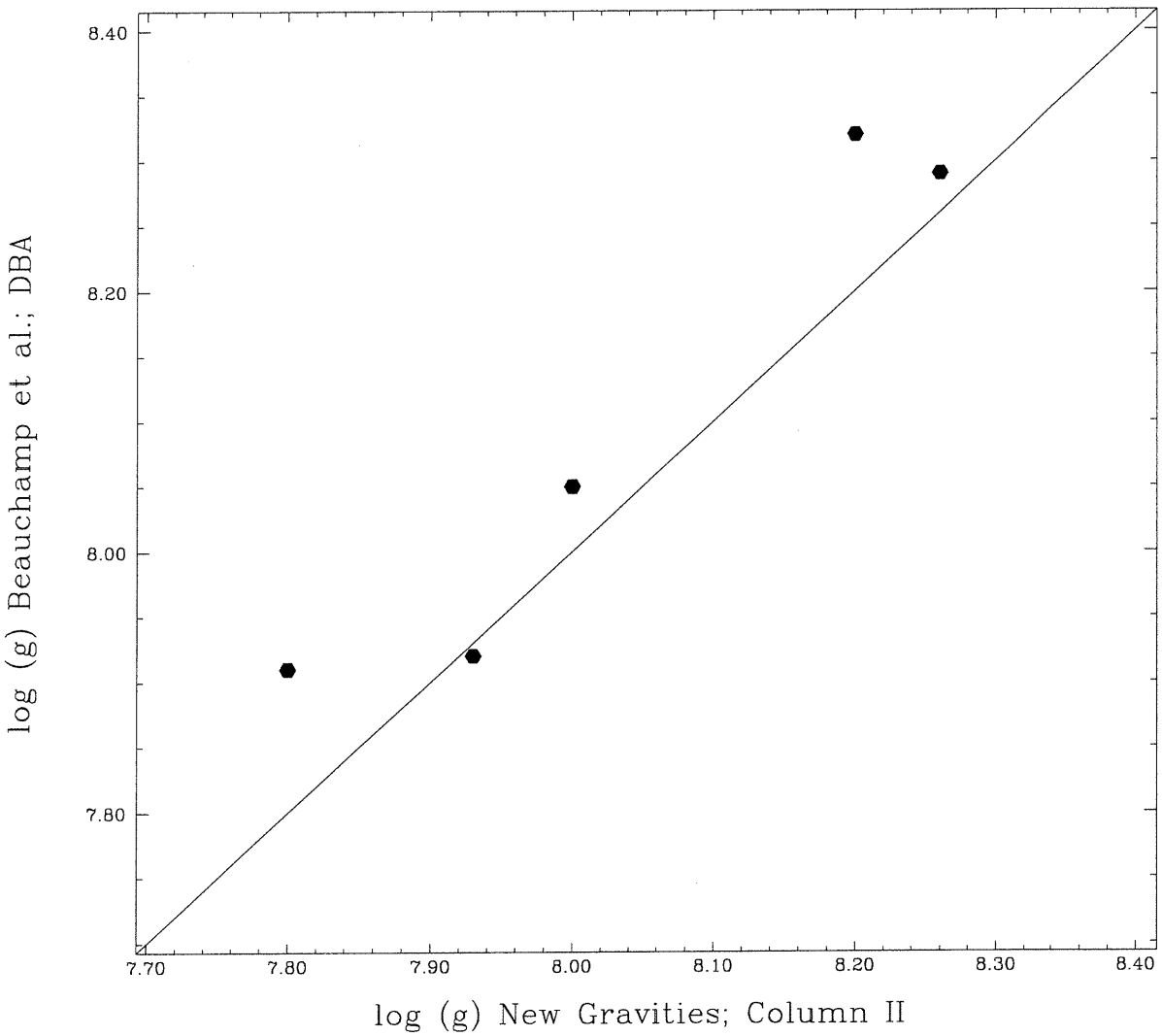

Figure 1.9: Comparison of gravities from DBA column of Table 1 in Beauchamp et al. (1999) with values derived from our new analysis using only blue spectra .

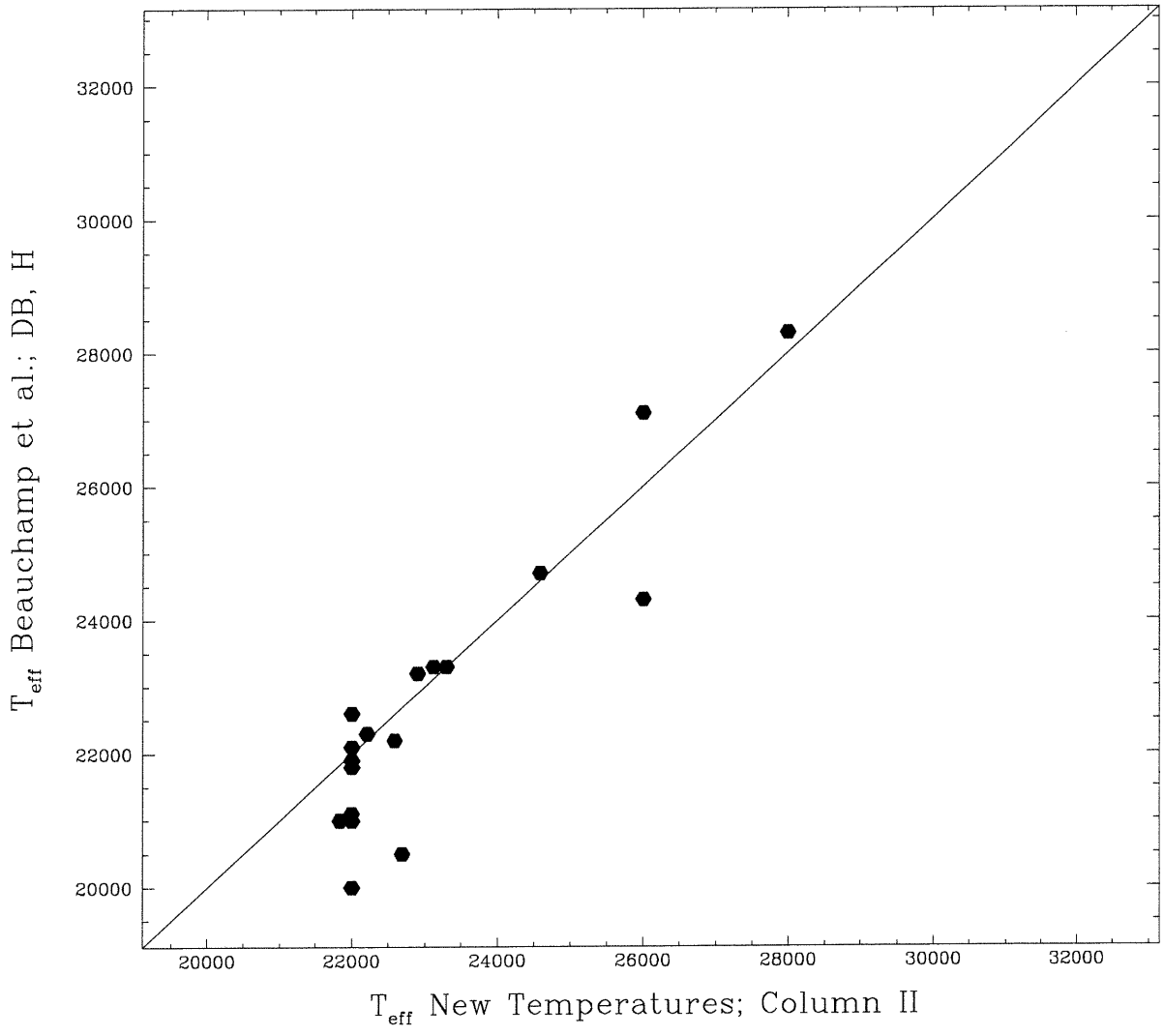

Figure 1.10: Comparison of temperatures from last column of Table 1 in Beauchamp et al. (1999) with values from our new analysis using only blue spectra. This figure is discussed in sec. 1.4.2. We have used the fixed same N(He)/N(H) values described in B99 to derive our temperatures.

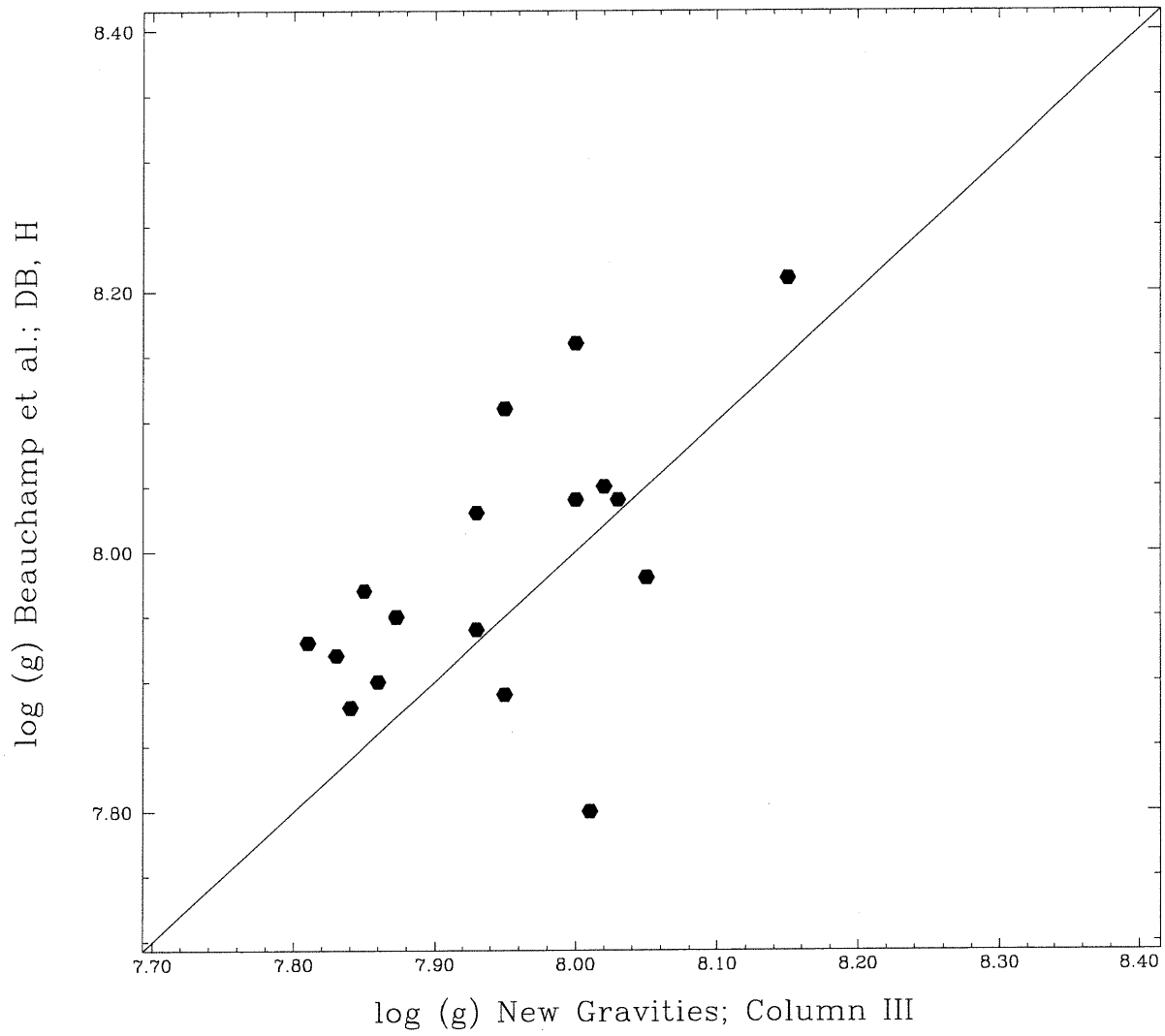

Figure 1.11: Comparison of gravities from last column of Table 1 in Beauchamp et al. (1999) with values derived from our new analysis using only blue spectra. Again, we see lower log g values than previously found.

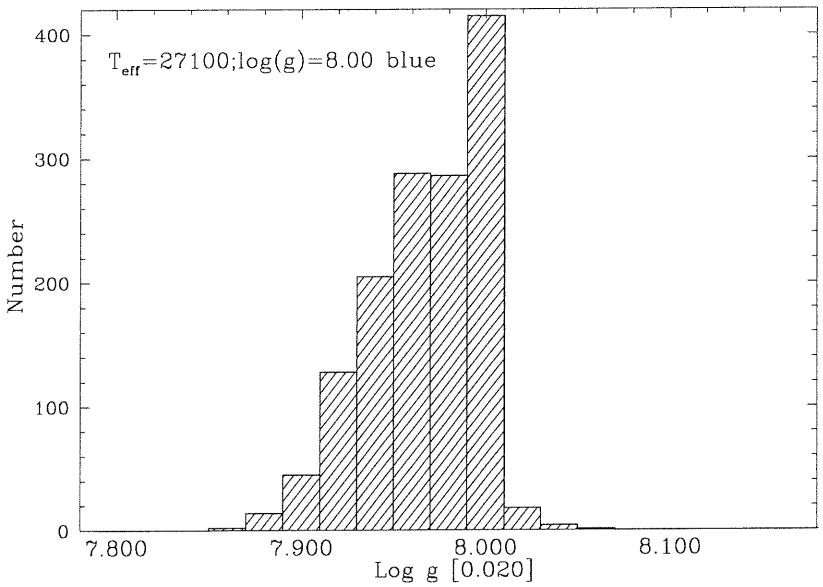

Figure 1.12: Histogram of gravities returned by simulated blue spectra with a S/N=65 in 0.02 dex bins. The skewed-ness of the distribution explains the divergent log g values reported in figs. 1.7 & 1.11. Ideally, we expect the distribution of artificial observations to be symmetric around the chosen surface gravity of the simulated spectra.

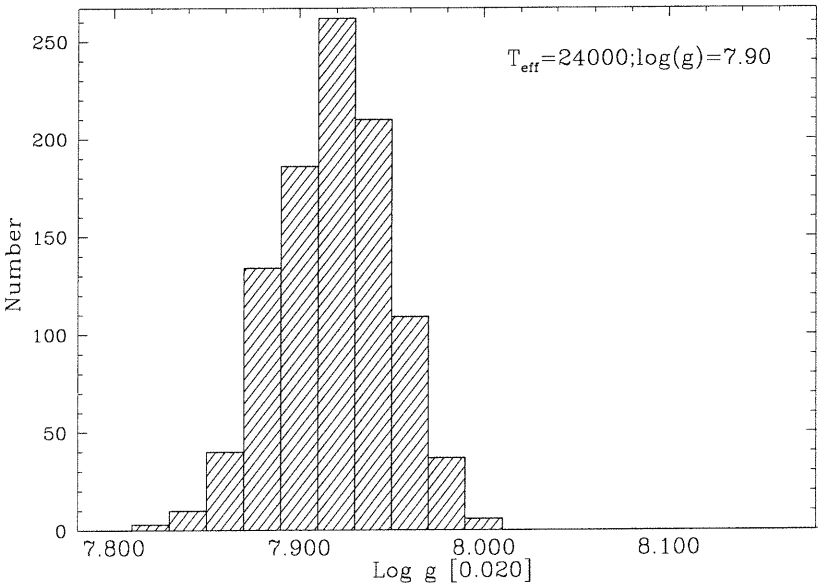

Figure 1.13: Histogram returned by combined blue + red fits with a S/N ratio of 100. The distribution appears relatively symmetric but is shifted to a higher values than original synthetic spectra.

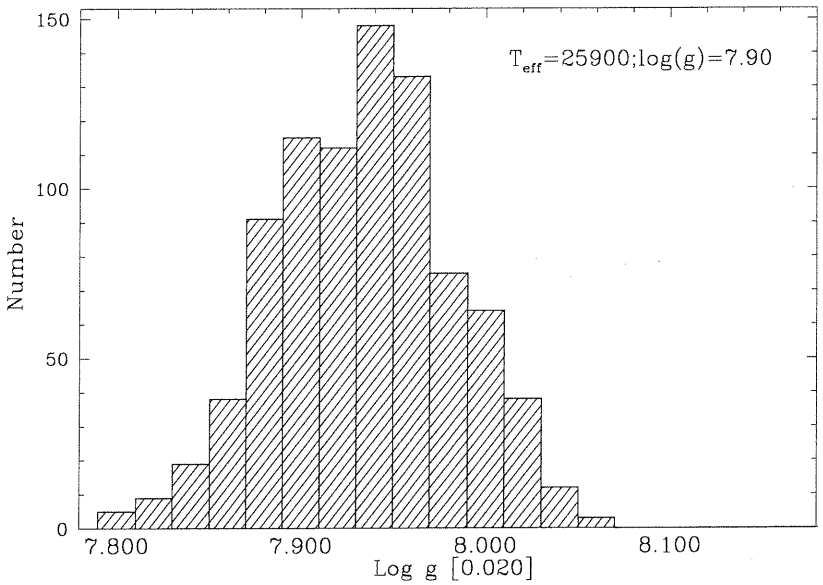

Figure 1.14: Histogram returned by combined blue + red fits with a S/N=50. The dispersion of results has increased from fig. 1.13 due to lower S/N ratio and the shift of the peak from the original value is larger.

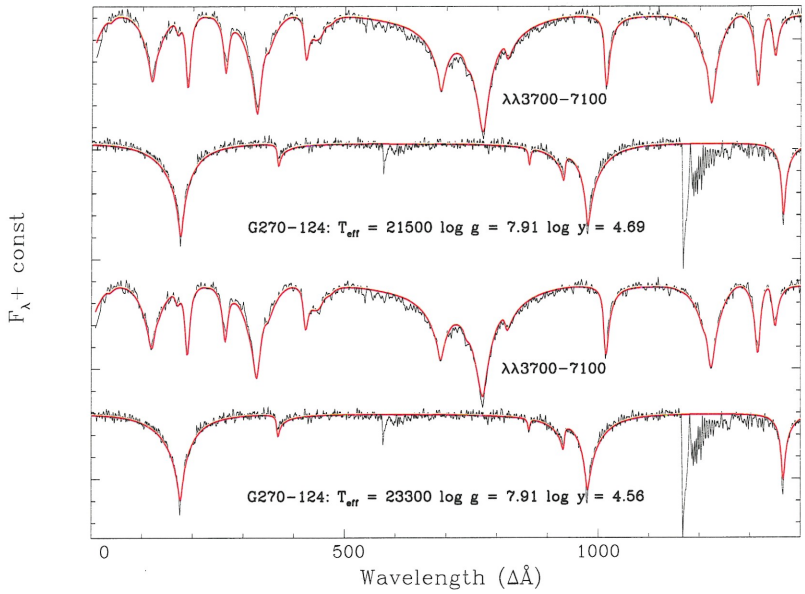

Figure 1.15: The two χ^2-minima solutions for G 270-124. Each solution has the spectra presented in two parts. The blue portion (upper spectra) starts at λ3700Å and the red portion starts with λ5700Å. The hotter solution has the lower χ^2 value, but the cooler solution appears to best describe the Hα profile.

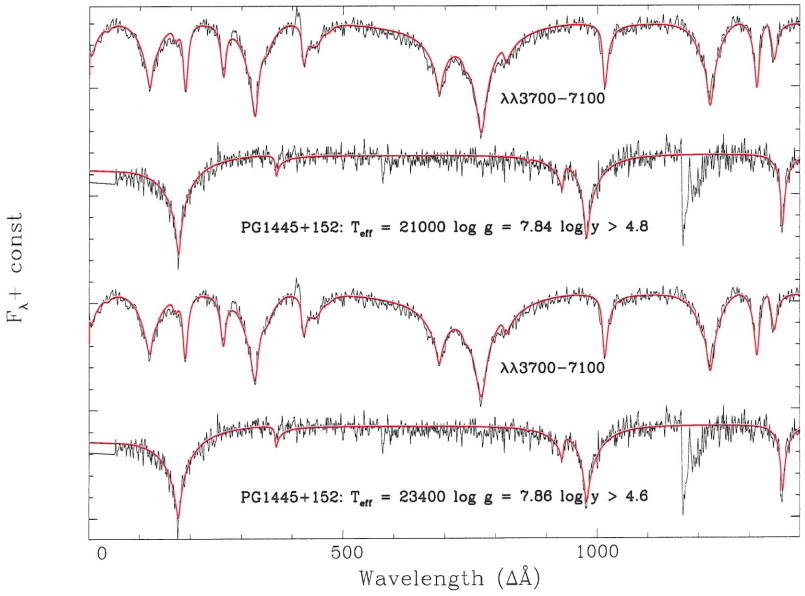

Figure 1.16: Two χ^2-minima for fits of PG 1445+152. Same format as G 270-124 in Fig. 1.15. Simulations indicate the two solutions overlap.

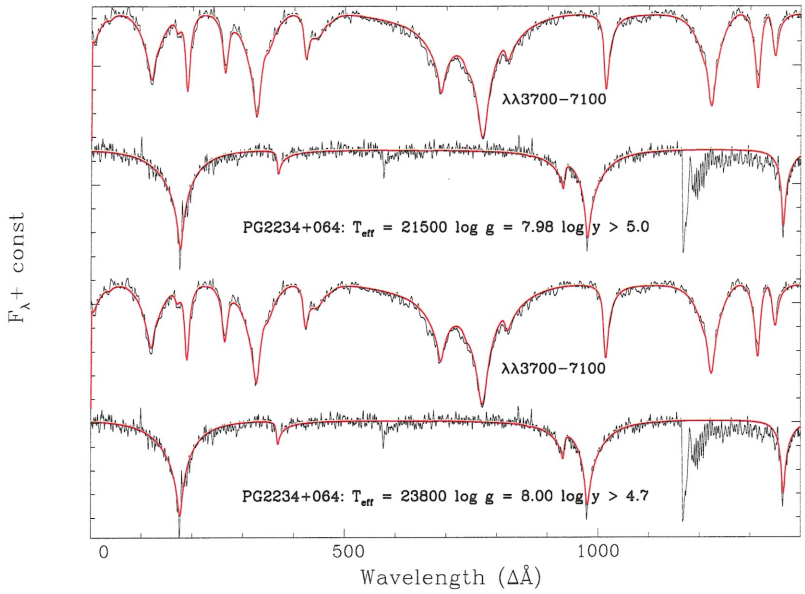

Figure 1.17: Two χ^2-minima for fits of PG 2234+064. Same format as Fig. 1.15 spectra start at λ3700Å and λ5700 Å.

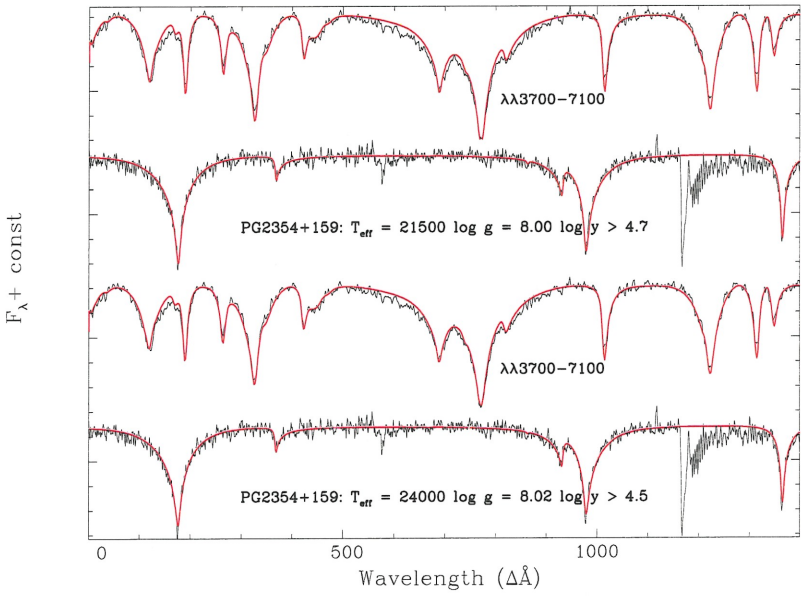

Figure 1.18: Two χ^2-minima for fits of PG 2354+159. Same format as Fig. 1.15 spectra start at λ3700Å and λ5700 Å.

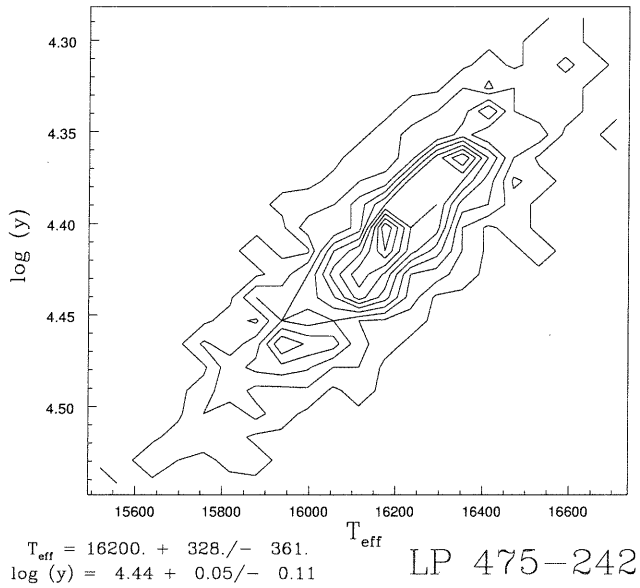

Figure 1.19: Simulation results for cool DBA LP 475-242. Note prominent $T_{\rm eff}$-log y relationship.

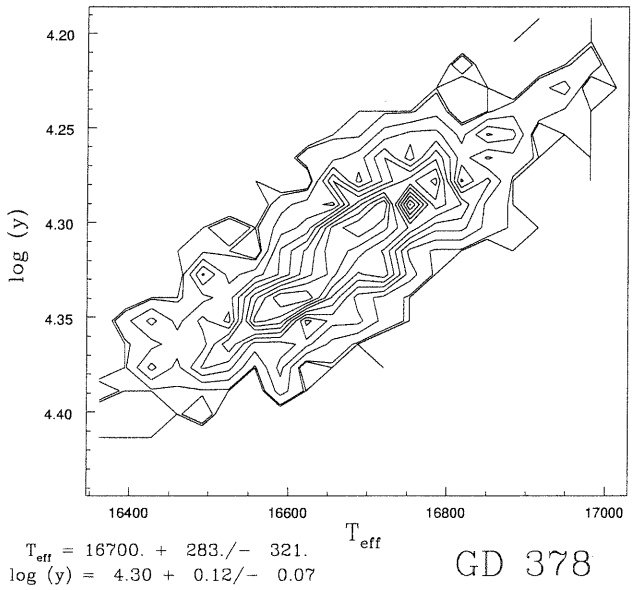

Figure 1.20: Simulation results for DBA GD 378

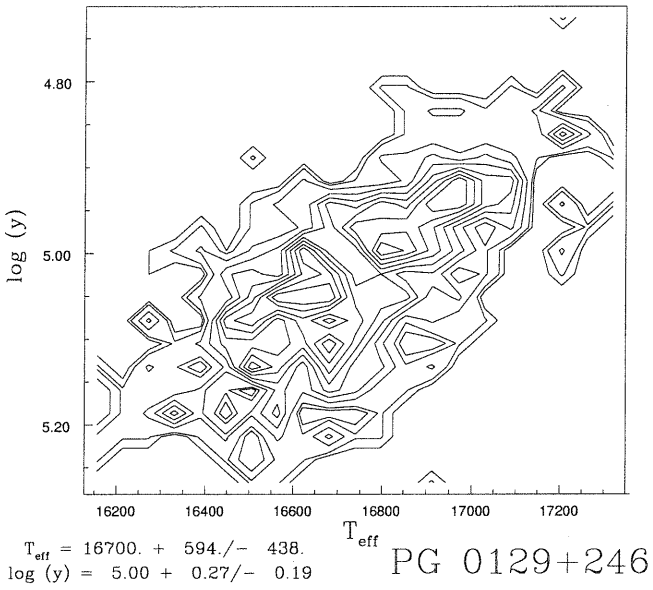

Figure 1.21: Simulation results for DBA PG 0129+246

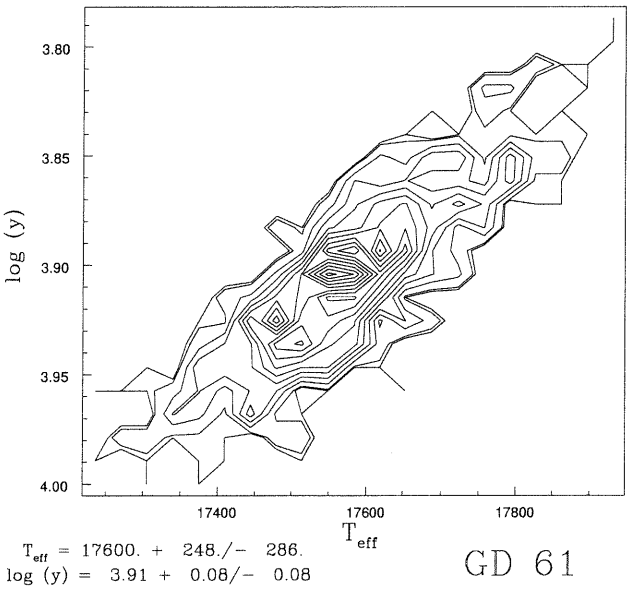

Figure 1.22: Simulation results for DBA GD 61

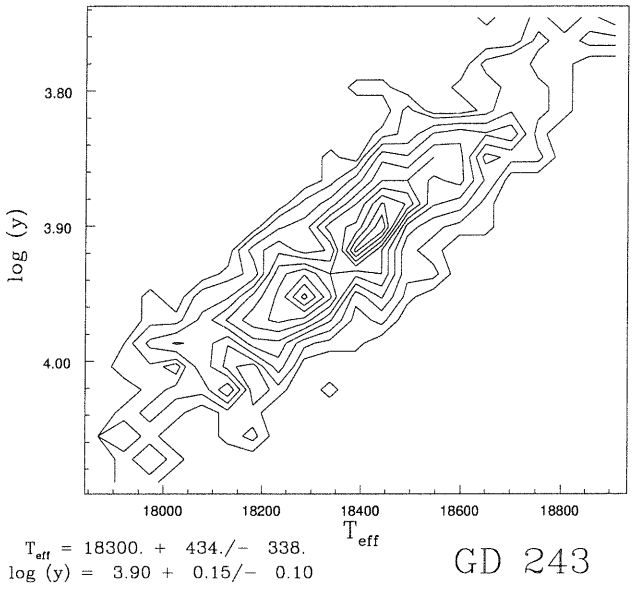

Figure 1.23: Simulation results for DBA GD 243

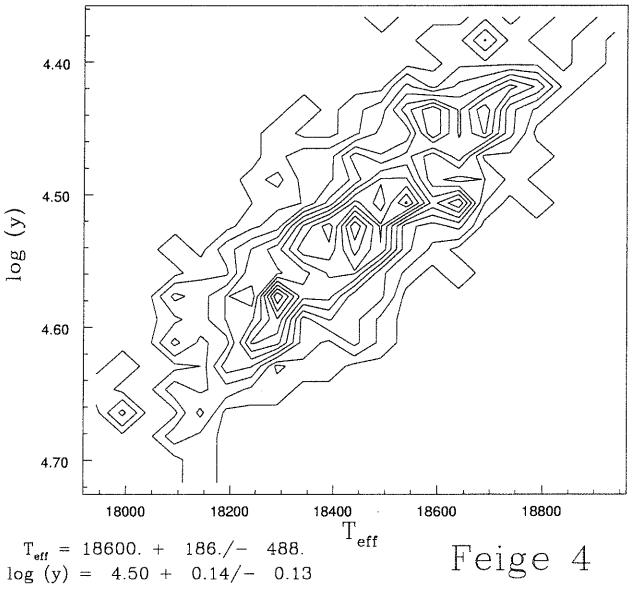

Figure 1.24: Simulation results for DBA Feige 4

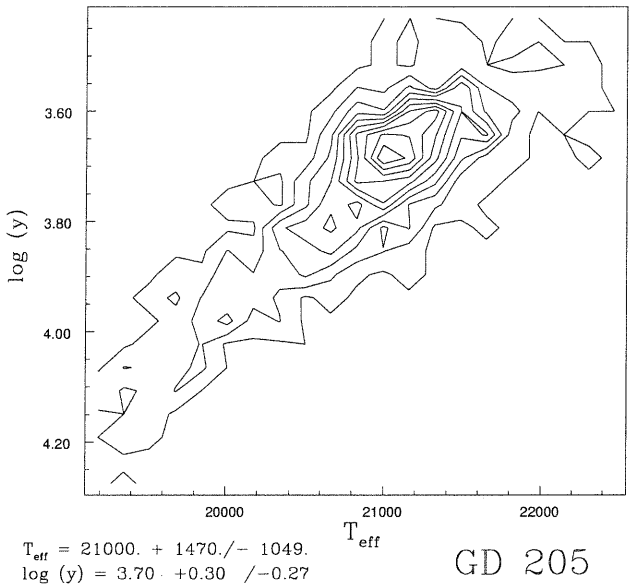

Figure 1.25: Simulation results for DBA GD 205

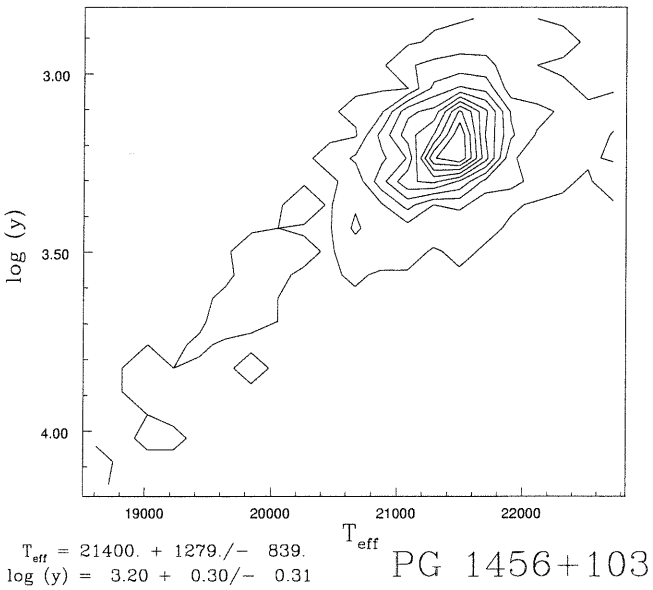

Figure 1.26: Simulation results for DBAV PG 1456+103

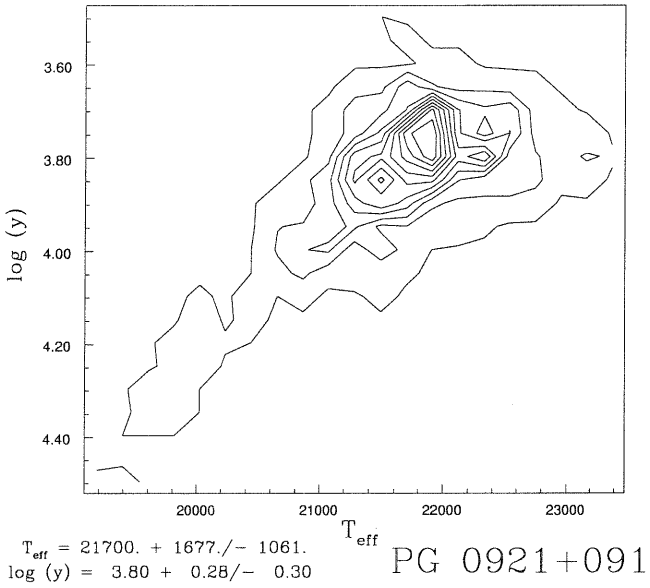

Figure 1.27: Simulation results for DBA PG 0921+091

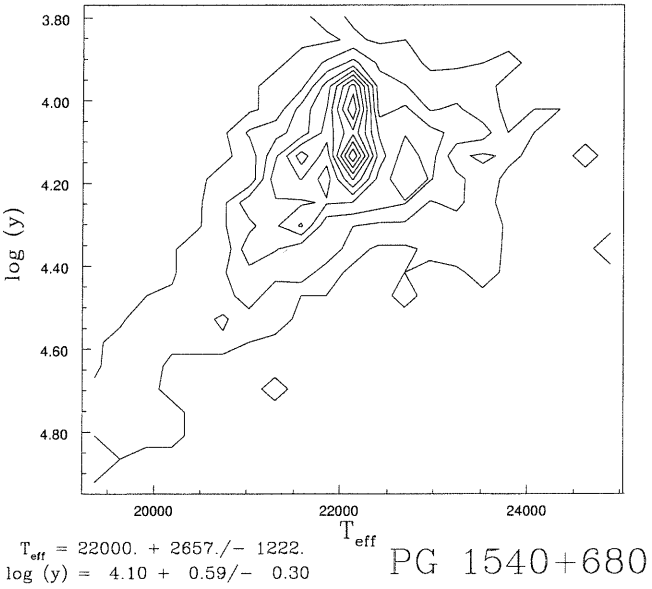

Figure 1.28: Simulation results for DBA PG 1540+680

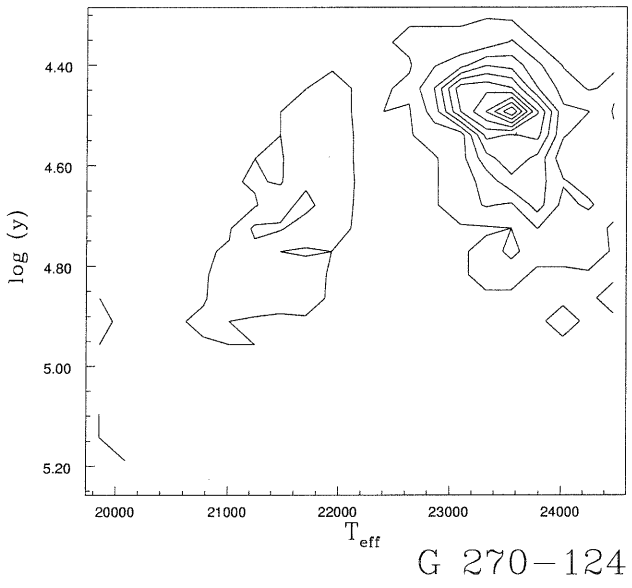

Figure 1.29: Contours for two solutions of DBA G 270-124

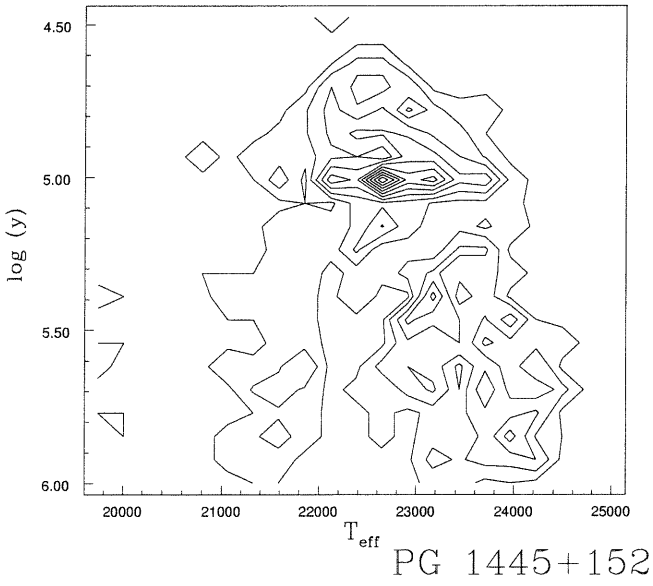

Figure 1.30: Simulation results for two solutions of DB PG 1445+152

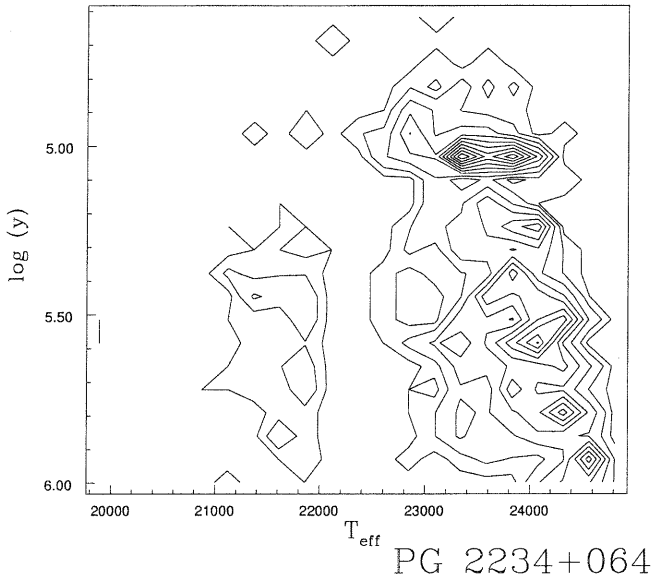

Figure 1.31: Contours for two solutions of DB PG 2234+064

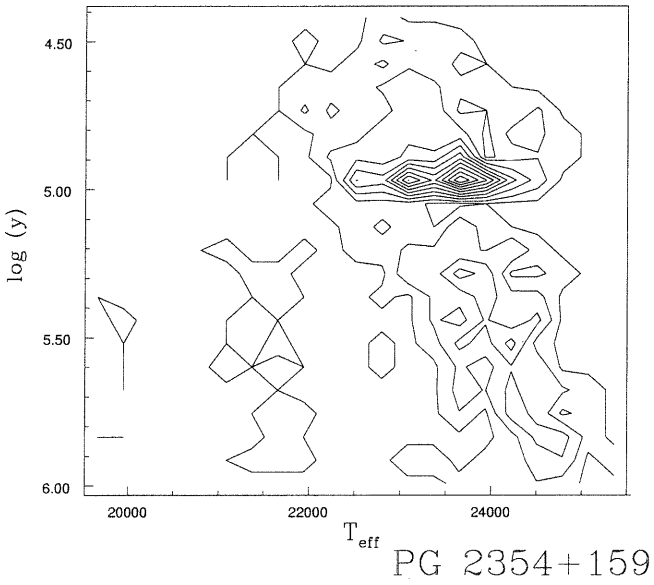

Figure 1.32: Simulation results for DB PG 2354+159

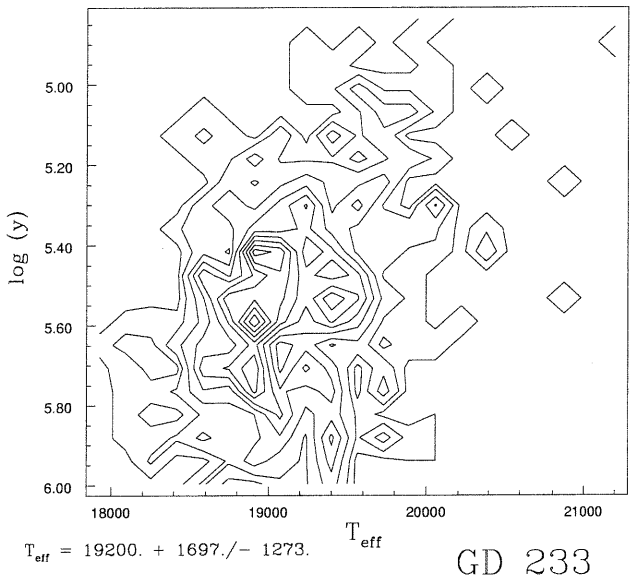

Figure 1.33: Contours for DB GD 233

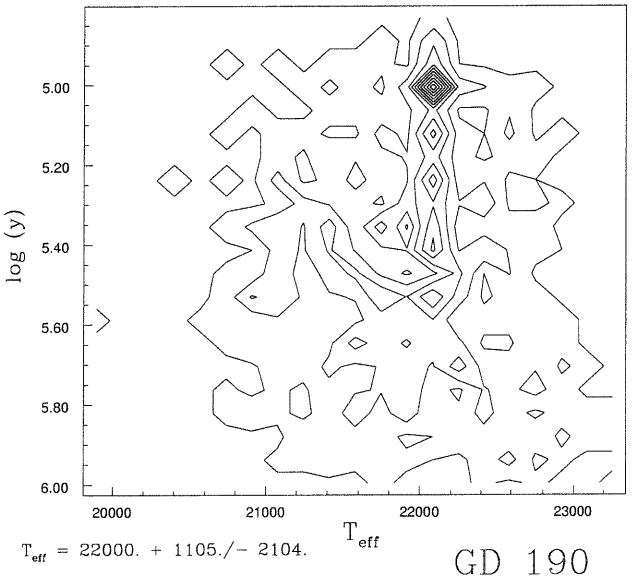

Figure 1.34: Simulation results for DB GD 190

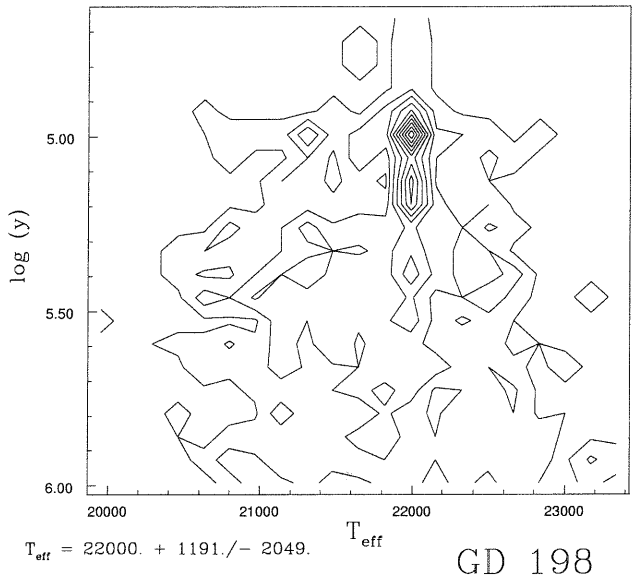

Figure 1.35: Contours for DB GD 198

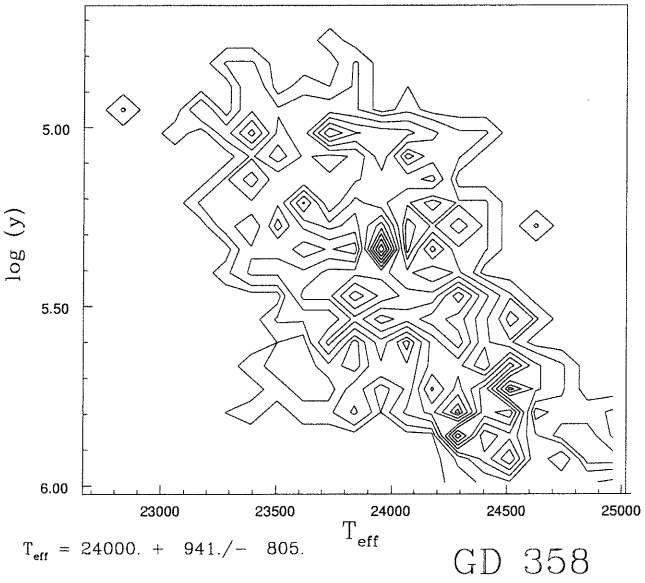

Figure 1.36: Simulation results for DBV GD 358

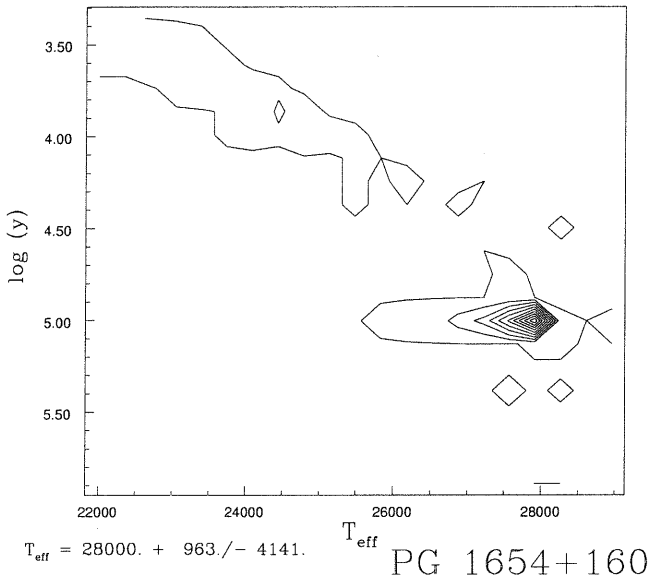

Figure 1.37: Simulation of blue spectra for DBV PG 1654+160

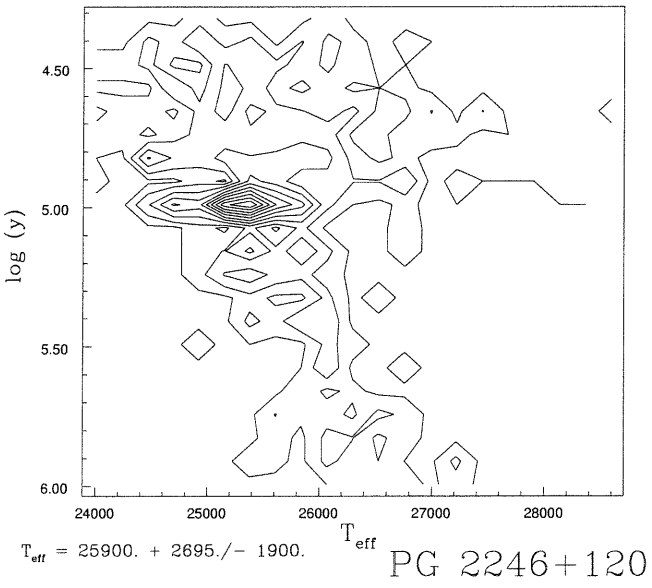

Figure 1.38: Contours for DBV PG 2246+120

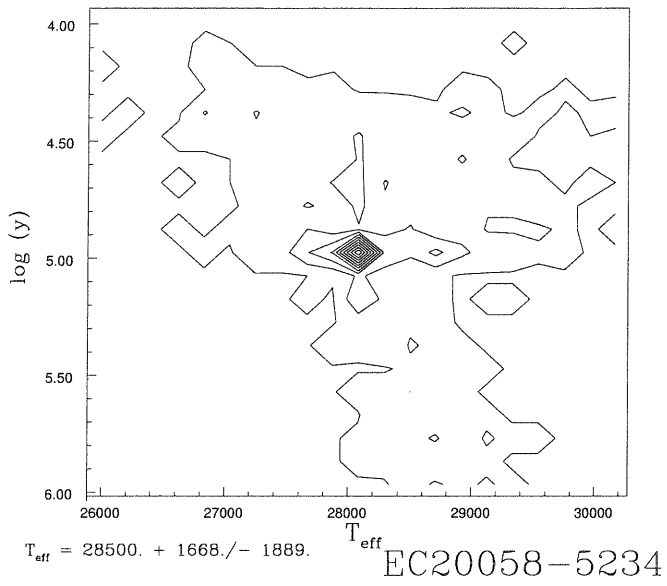

Figure 1.39: Contours for DBV EC20058-5234

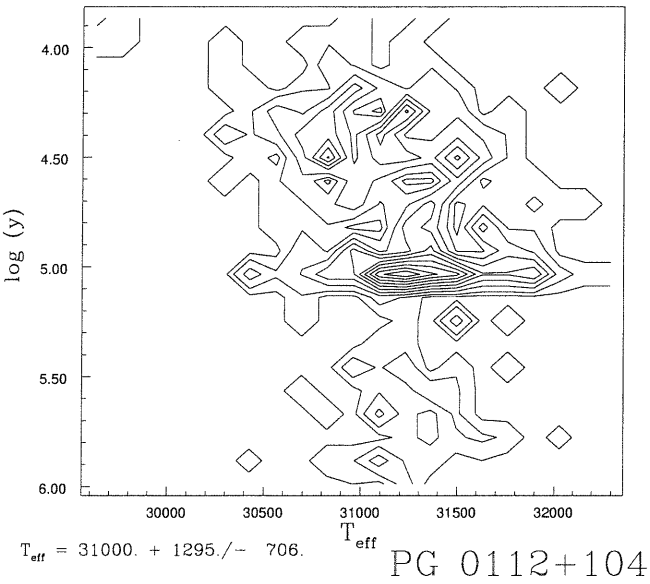

Figure 1.40: Simulation results for DB PG 0112+104

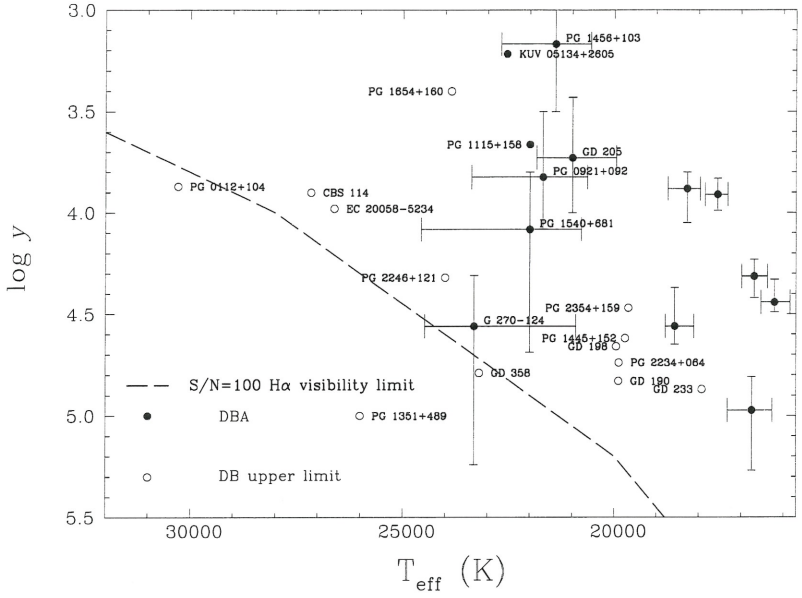

Figure 1.41: Upper limits and abundance ratios for our results in table 1.3. Error bars for G 270-124 cover both solutions listed. Open circles are upper limits for Balmer line non-detections using the lowest temperatures/smallest log y from the error limits. Constraining hydrogen further will shift these open circles down and to the left on this graph. The DBA stars (solid points) below 20,000K have smaller errors as we expect from the increased response of He I optical lines. The dashed line is the estimated detection threshold for Hα assuming a S/N ratio of 100. As indicated we currently cannot rule out the hottest DB stars having log y=4.0, the typical abundance ratio of DBA white dwarfs.

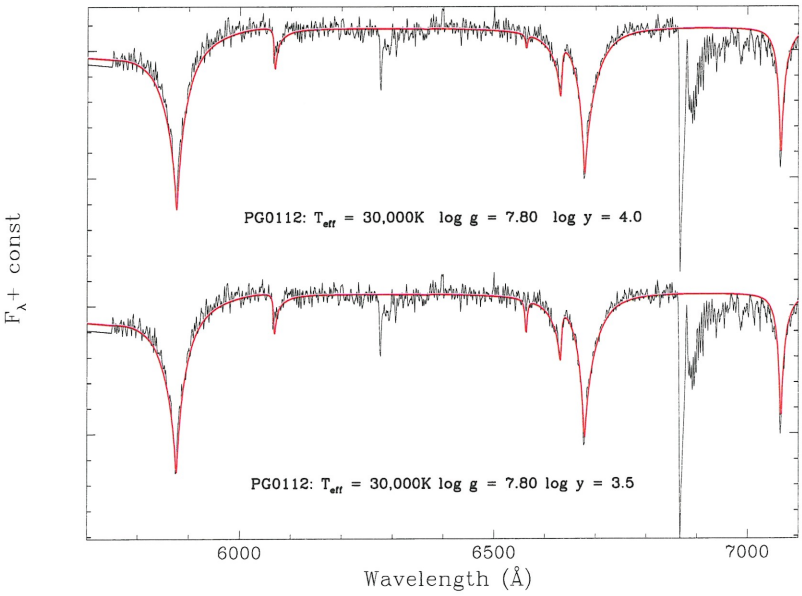

Figure 1.42: Using atmosphere values similar to Provencal et al. (2000) we can rule out the upper portion of their quoted range of N(He)/N(H) ratio. We do not confirm detection of hydrogen in PG 0112+104. We cannot rule out log y~4.0 from our spectra. The feature at λ6680Å is the terrestrial O_2 B-band.

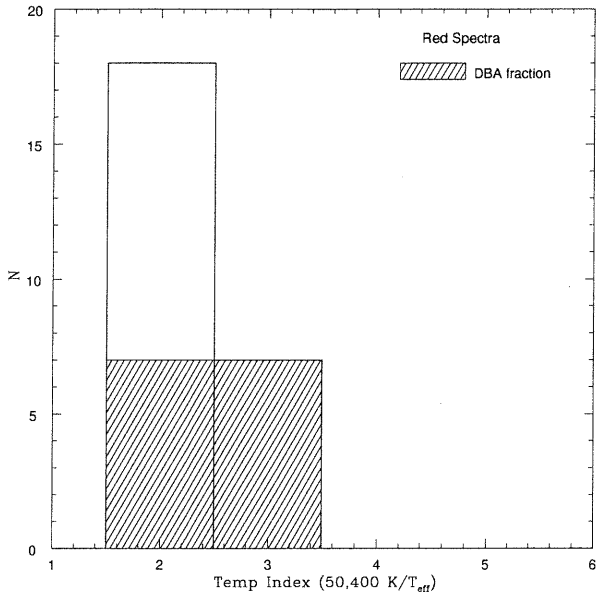

Figure 1.43: DBA fraction for hot DB2 stars from Hα and our sub-sample of DBA3 white dwarfs.

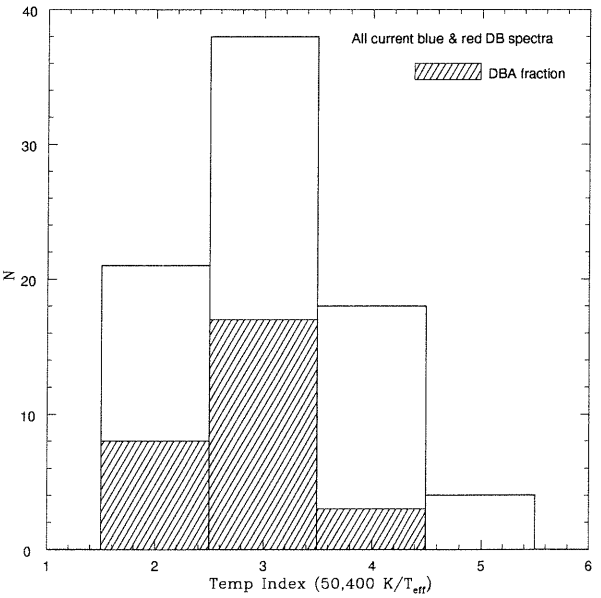

Figure 1.44: DBA fraction of all our current spectra covering Hα (DB2) and Hβ (DB3). Our sample contains 21 DB2 stars while the McCook & Sion catalog lists 13. In addition to the 18 hot DB white dwarfs in this study, we have included PG 1326-037, LP 497-114, LB 8827 (Beauchamp et al. 1999; Wesemael et al. 2001; Wickramasinghe & Reid 1983). The McCook & Sion catalog lists 61 DB3 + DB4 objects (fig. 1.1) our spectra database has 56 stars in these two bins.

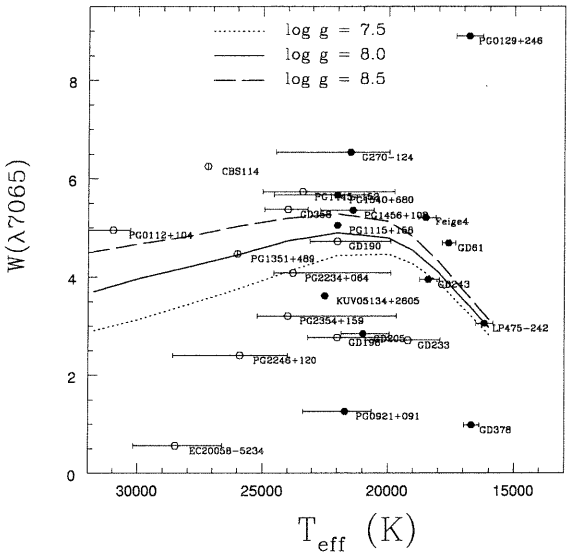

Figure 1.45: Measured equivalent widths (points) and theoretical widths (lines). Noise dominates over the measured equivalent width of this profile. The solid points are DBA stars. EC20058-5234 suffers from sensitivity problems which has reduced the equivalent width.

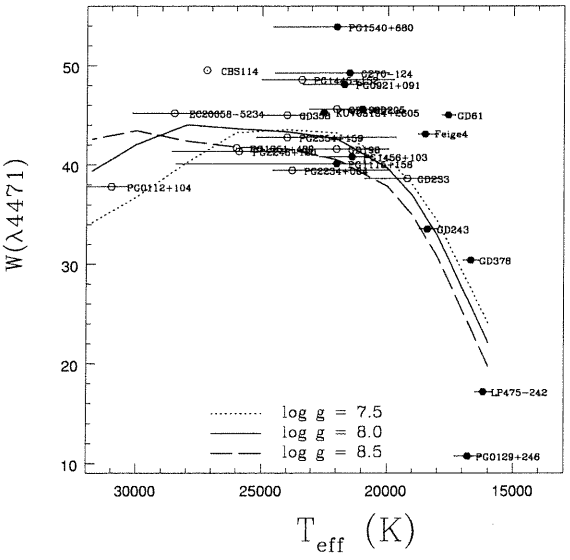

Figure 1.46: Measured equivalent widths (points) and theoretical widths (lines) for the group of lines λ4387+4471+4517. The scatter here is due to noise in the spectra. We see that many points lie above the theoretical values, especially near 22,000K. This may indicate our measurement technique introduces a bias to the estimated equivalent widths.

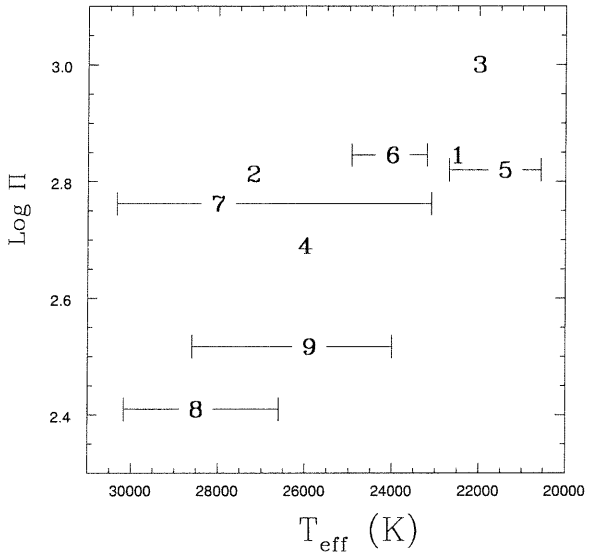

Figure 1.47: Log of period v/s effective temperature for pulsating DB white dwarfs. Pulsation periods & ordinals are from table 1.1, temperatures and error bars are from table 1.3. The uncertainties of the four numerals without error bars are similar to PG 1654+160(7). The choice of the dominant period is uncertain, particularly for the coolest objects therefore, the uncertainty for the periods will be large. Periods with least uncertainty are EC20058-5234(8), PG 2246+120(9), PG 1351+489(4) & GD358(6).

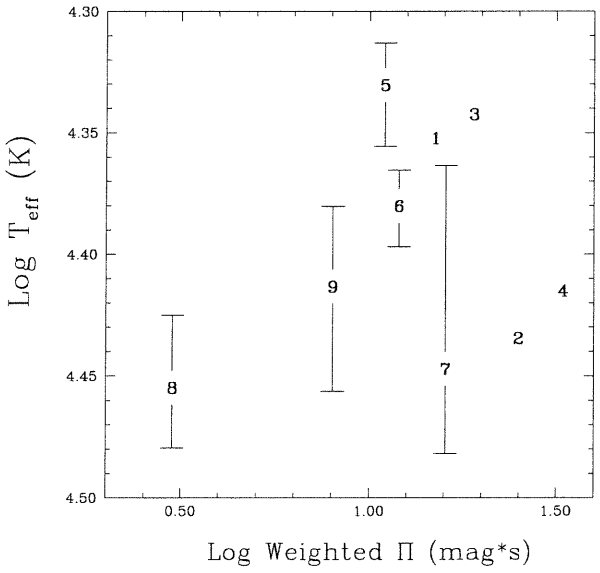

Figure 1.48: Weighted period v/s temperature for DBV stars. Pulsation periods are multiplied by the mode amplitude. Assuming temperature and pulsation power are proportional, this graph can be compared to fig. 6b in Koen et al. (1995). Similar to fig. 1.47, there is large uncertainty in the choice of dominant period.

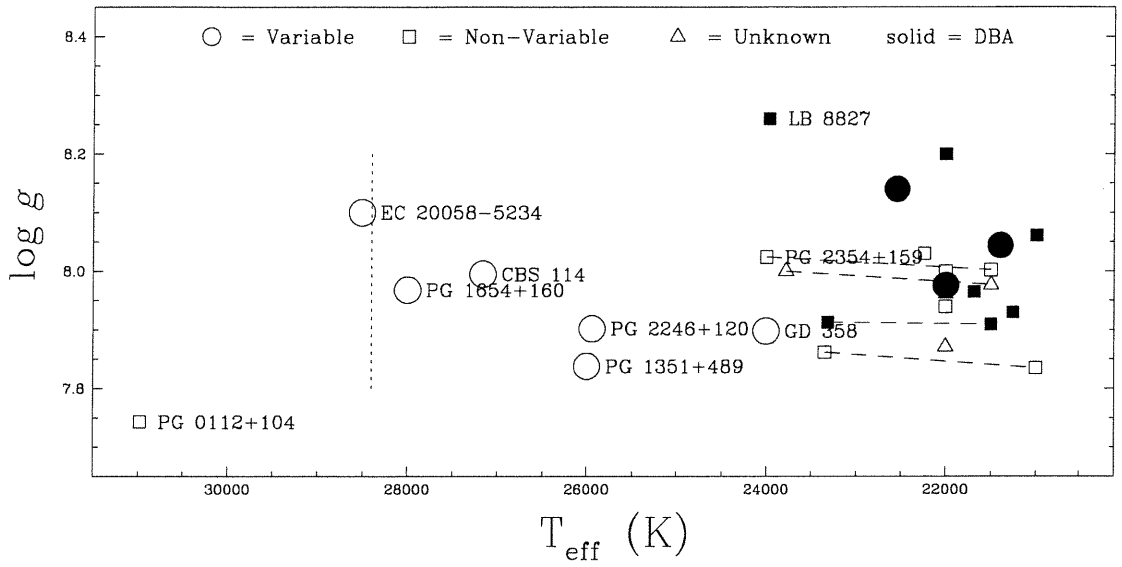

Figure 1.49: The observed instability strip. The four stars with two possible solutions (sec. 1.5.2) are connected by dashed lines. Note that the DBA variables appear to occupy a temperature range separate from the helium DBV stars. The peculiar magnetic white dwarf LB 8827 may be the only non-pulsating DBA occupying the DBV range of the instability strip. The vertical line locates the blue edge from non-adiabatic theory (Brassard & Fontaine 1997a) for log g =8.0. DBA white dwarfs are solid points while DB stars are open symbols. Several of the cooler DBA stars on this diagram are identified as non-variable from the unpublished observations of G. Handler (private communication)

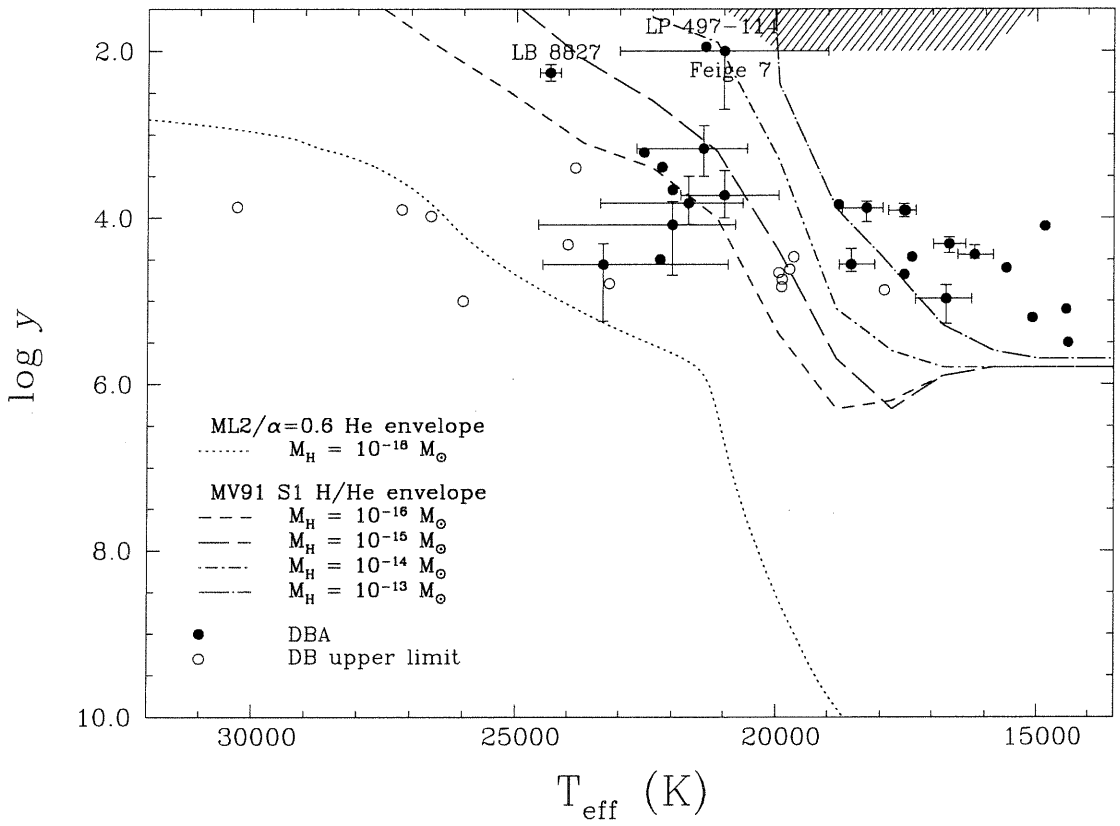

Figure 1.50: We plot abundance H/He ratio for 30 DBA stars in our database of DB spectra. We also plot upper limits from red spectra for non-detections of Hα . The dotted line uses the ML2/α =0.6 atmosphere of Fontaine et al. (2001) with $M_H = 10^{-18}M_\odot$ of hydrogen uniformly mixed throughout. Other hydrogen masses will shift this curve vertically. This plot indicates that four DB white dwarfs have hydrogen mass upper limits near $10^-18M_\odot$. Dashed lines indicate models of MV91 which have explicitly accounted for poisoning of the helium convection zone from hydrogen. There is significant difference in the photospheric abundance ratio below 20,000K for these two models. Unlike the ML2 case, the evolution of the helium convection zone is dependent on hydrogen content for the models in MV91 particularly below 18,000K where the convection zone has been almost completely saturated by the more opaque hydrogen. MV91 models use the Schwarzschild mixing length prescription. The hatched region in the upper right corner is their unstable region where they expect a discontinuous jump in photospheric abundances.

Conclusion

Nous avons combiné un ensemble de spectres rouges (λ5700Å-λ7200Å) avec des spectres bleus (λ3400Å-λ5000Å) obtenus précédemment afin d'étudier les patrons d'abondance d'hydrogène dans les étoiles naines blanches chaudes de type DB (photosphère riche en hélium). Les nouveaux spectres, qui sont centrés sur la raie Hα de l'hydrogène atomique, nous procurent une sensibilité aux petites quantités d'hydrogène dans l'atmosphères de ces étoiles.

Les nouveaux modèles d'atmosphère contenant à la fois hydrogène et hélium nous permettent d'obtenir une limite de log $y \gtrsim 4.0$ pour l'étoile DB la plus chaude, PG 0112+104. Nous plaçons également une limite de log $y \gtrsim 4.8$ dans l'étoile pulsante GD 358. Ces limites sont en bon accord avec les resultats de PSTV00 à partir la spectroscopie de Lyman-α. Avec l'étude précedente de SLG87, nous pouvons conclure que les naines blanches DBA ont une abondance typique de log y =4.0 dans l'interval de températures effectives entre 22,000K et 14,000K.

Au sein de l'échantillon observé dans le cadre de ce projet, 10 étoiles sont de sous-type DBA, avec une abondance typique de log y ~4.0. Au moins de deux ces objets possèdent un champ magnetique. Nous obtenons, pour les étoiles DB chaudes où nous n'avons pas détecté de raies de Balmer, également une limite supérieure log $y \gtrsim 4.0$.

Une fois l'abondance d'hydrogène connue, une redétermination autocohérente de l'échelle de température des étoiles DB chaudes a été complétée. Nos nouvelles températures impliquent que la bande d'instabilité empirique s'étend approximativement de 28,000K à 21,000K. Nous avons trouvé que les trois étoiles DB pulsantes les plus froides contiennent de l'hydrogène. Les étoiles pulsantes DBAV semblent donc être caractérisées par des températures inférieures à celles des DBV. Les variables DBV sont restreintes à une gamme de températures effectives entre 28,000K et 24,000K, alors que les DBAV occupent la région entre 22,500K et 21,000K.

Une analyse plus détaillée serait requise pour confirmer que le côté bleu de la bande d'instabilité des étoiles DBA est plus froid que celui des étoiles DB. Nos résultats suggèrent que la bande d'instabilité des variables DBV est pure, et ne contient pas d'étoiles non pulsantes.

Notre technique de fit non-linéaire a des difficultés considérables avec les spectres dont les raies d'hélium neutre sont proches de leur élargissement maximal. Les températures des étoiles dans la gamme 21,000K - 24,000K demeurent donc incertaines. Pour quatre étoiles de notre échantillon, une ambiguïté persiste dans la détermination de la température effective, et nous ne ne sommes pas capables de choisir entre deux températures possibles.

Nous avons utilisé des simulations du type Monte Carlo pour détérminer la fiabilité de nos résultats. Les étoiles chaudes ont les plus grandes incertitudes sur leurs températures. Nous avons aussi trouvé que les erreurs sur l'abondance d'hydrogène sont fortement dépendantes de la qualité du spectre et de l'intensité de la raie Hα .

Nous remarquons que les incertitudes pour les DBA suivent une relation log-linéaire entre l'abondance, log y et la température effective, $T_{\rm eff}$. En comparant avec nos resultats précédents provenant des spectres bleus seulement, nos nouvelles gravités de surface différent systematiquement des anciennes valeurs. Nous avons mesuré les largeurs equivalentes des raies λ4471Å et λ7065Å. Le maximum de la largeur equivalente se trouve près de 22,000K, ce qui est en accord avec la théorie de longueur de mélange (TLM) dans sa version ML2.

Nous avons derivé des quantités totales d'hydrogène dans chaque objet en utilisant des modèles construits à l'aide de la paramétrisation ML2 de la TLM. Nos masses sont similaires à celles de PSTV00. Au moins quatre de nos étoiles DB chaudes ne semblent pas avoir une masse d'hydrogène suffisante pour pouvoir avor été une naine blanche DA riche en hydrogène lors de sa traversée de la brèche des DB.

Nous comparons les plus récents modèles d'enveloppe d'hélium, qui utilisent la TLM ML2 avec les modèles d'enveloppes plus anciens à composition mixte d'hydrogène et d'hélium. Ces modèles plus anciens tiennent compte des effets d'opacité d'hydrogène dans l'enveloppe. Ces effets sont importants, cars ils représentent le lien entre la masse de la zone convective et la quantité d'hydrogène dans l'enveloppe. Aucun des deux modéles ne peut expliquer l'évolution des abondances observées dans les naines blanches DBA. Nous avons trouvé une

masses moyenne d'hydrogène de $M_H = 10^{-13} M_\odot$ pour les objets DBA3, et une masse moyenne de $M_H = 10^{-16} M_\odot$ pour les DBA2.

Afin d'expliquer les abondances des étoiles DBA, il faut faire l'hypothèse que les étoiles DB accrètent l'hydrogène du milieu interstellaire. Nous estimons qu'un taux d'accretion de $\dot{M}_H = 10^{-21} M_\odot$/an est nécessaire afin d'expliquer les abondances des naines blanches DBA2 et DBA3. Ce taux d'accretion est plus faible que celui trouvé dans les études antérieures.

Bibliographie

Aannestad, P. A. & Sion, E. M. 1985, AJ, 90, 1832

Achilleos, N., Wickramasinghe, D. T., Liebert, J., Saffer, R. A., & Grauer, A. D. 1992, ApJ, 396, 273

Beauchamp, A. 1995, PhD thesis, Université de Montréal

Beauchamp, A., Wesemael, F., & Bergeron, P. 1997, ApJS, 108, 559

Beauchamp, A., Wesemael, F., Bergeron, P., Fontaine, G., Saffer, R. A., Liebert, J., & Brassard, P. 1999, ApJ, 516, 887, (B99)

Beauchamp, A., Wesemael, F., Bergeron, P., & Liebert, J. 1995a, ApJ, 441, L85

Beauchamp, A., Wesemael, F., Bergeron, P., Liebert, J., & Saffer, R. A. 1996, in ASP Conf. Ser. 96: Hydrogen Deficient Stars, 295

Beauchamp, A., Wesemael, F., Bergeron, P., Saffer, R. A., & Liebert, J. 1995b, in LNP Vol. 443: White Dwarfs, 108

Bergeron, P., Saffer, R. A., & Liebert, J. 1992, ApJ, 394, 228, (BSL92)

Bergeron, P., Wesemael, F., Lamontagne, R., Fontaine, G., Saffer, R. A., & Allard, N. F. 1995, ApJ, 449, 258

Bergeron, P., Wesemael, F., & Saffer, R. A. 2000, PASP, 112, 837

Böhm-Vitense, E. 1992, Stellar Astrophysics: Stellar Structure and Evolution, Vol. 3 (Cambridge University Press)

Bradley, P. A., Winget, D. E., & Wood, M. A. 1993, ApJ, 406, 661, (BWW93)

Brassard, P. & Fontaine, G. 1997a, in ASSL Vol. 214: White dwarfs, 451

Brassard, P. & Fontaine, G. 1997b, in The Third Conference on Faint Blue Stars, 485

Clemens, J. C., Barstow, M. A., Nather, R. E., Winget, D. E., Bradley, P. A., Claver, C. F., Dixon, J. S., Kanaan, A., Kleinman, S. J., Provencal, J., Wood, M. A., Sullivan, D., Wickramasinghe, D. T., Ferrario, L., Marar, T. M. K., Seetha, S., Ashoka, B. N., Leibowitz, E., Mendelson, H., O'Donoghue, D., Buckley, D. A., Chen, A.-L., Zola, S., Krzesinski, J., Moskalik, P., Vauclair, G., Fremy, J.-R., Chevreton, M., Kepler, S. O., & Odilon, G. 1993, in NATO ASIC Proc. 403: White Dwarfs: Advances in Observation and Theory, 515+

D'Antona, F. & Mazzitelli, I. 1979, A&A, 74, 161

Daou, D., Wesemael, F., Fontaine, G., Bergeron, P., & Holberg, J. B. 1990, ApJ, 364, 242

Dappen, W., Anderson, L., & Mihalas, D. 1987, ApJ, 319, 195

Dupuis, J., Fontaine, G., & Wesemael, F. 1993, ApJS, 87, 345

Dupuis, J., Pelletier, C., Fontaine, G., & Wesemael, F. 1987, in IAU Colloq. 95: Second Conference on Faint Blue Stars, 657

Eggen, O. J. & Greenstein, J. L. 1965, ApJ, 141, 83

Fontaine, G., Brassard, P., & Bergeron, P. 2001, PASP, 113, 409

Fontaine, G., Tassoul, M., & Wesemael, F. 1987, in IAU Colloquium No 95., The Second Conference on Faint Blue stars, 657

Green, R. F., Schmidt, M., & Liebert, J. 1986, ApJS, 61, 305

Handler, G. 2001, MNRAS, 323, L43

Hansen, B. M. S. 1999, ApJ, 520, 680

Hansen, C. J., Winget, D. E., & Kawaler, S. D. 1985, ApJ, 297, 544

Hummer, D. G. & Mihalas, D. 1988, ApJ, 331, 794

Hunter, C., Wesemael, F., Saffer, R. A., Bergeron, P., & Beauchamp, A. 2001, in 12th European Workshop on White Dwarfs, in press (HWSBB01)

Kawaler, S. D., Winget, D. E., & Hansen, C. J. 1985, ApJ, 298, 752

Kepler, S. O. & Nelan, E. P. 1993, AJ, 105, 608

Kepler, S. O., Robinson, E. L., Koester, D., Clemens, J. C., Nather, R. E., & Jiang, X. J. 2000, ApJ, 539, 379

Koen, C., O'Donoghue, D., Stobie, R. S., Kilkenny, D., & Ashley, R. 1995, MNRAS, 277, 913

Koester, D. 1991, in NATO ASIC Proc. 336: White Dwarfs, 343

Koester, D. & Weidemann, V. 1989, A&A, 219, 276

Koester, D. & Wolff, B. 2000, A&A, 357, 587

Liebert, J. 1986, in ASSL Vol. 128: IAU Colloq. 87: Hydrogen Deficient Stars and Related Objects, 367

Liebert, J., Fontaine, G., & Wesemael, F. 1987, Memorie della Societa Astronomica Italiana, 58, 17

MacDonald, J. & Vennes, S. 1991, ApJ, 371, 719, (MV91)

McCook, G. P. & Sion, E. M. 1999, ApJS, 121, 1

Metcalfe, T. S., Nather, R. E., & Winget, D. E. 2000, ApJ, 545, 974

Michaud, G., Fontaine, G., & Charland, Y. 1984, ApJ, 280, 247

Napiwotzki, R. 1999, A&A, 350, 101

Nitta, A., Winget, D. E., Kepler, S. O., & et al. 1999, in ASP Conf. Ser. 169: 11th European Workshop on White Dwarfs, 104

Pelletier, C. 1986, PhD thesis, Université de Montréal

Pelletier, C., Fontaine, G., & Wesemael, F. 1989, in IAU Colloq. 114: White Dwarfs, 249

Press, W., Flannery, B., Teukolsky, S., & Vetterling, W. 1989, Numerical Recipes, 2nd edn. (Cambridge Univ. Press)

Provencal, J. L., Shipman, H. L., Thejll, P., & Vennes, S. . 2000, ApJ, 542, 1041, (PSTV00)

Robinson, E. L. & Winget, D. E. 1983, PASP, 95, 386

Saffer, R. A., Liebert, J., & Olszewski, E. W. 1988, ApJ, 334, 947

Shipman, H. L., Liebert, J., & Green, R. F. 1987, ApJ, 315, 239, (SLG87)

Sion, E. M. 1984, ApJ, 282, 612

Sion, E. M., Greenstein, J. L., Landstreet, J. D., Liebert, J., Shipman, H. L., & Wegner, G. A. 1983, ApJ, 269, 253

Thejll, P., Vennes, S., & Shipman, H. L. 1991a, ApJ, 370, 355

Thejll, P., Vennes, S., & Shipman, H. L. 1991b, in NATO ASIC Proc. 336: White Dwarfs, 257

Vuille, F., O'Donoghue, D., Buckley, D. A. H., Massacand, C.-M., Solheim, J. E., Bard, S., Vauclair, G., Giovannini, O., Kepler, S. O., Kanaan, A., Provencal, J. L., Wood, M. A., Clemens, J. C., Kleinman, S. J., O'Brien, M. S., Nather, R. E., Winget, D. E., Nitta, A., Klumpe, E. W., Montgomery, M. H., Watson, T. K., Bradley, P. A., Sullivan, D. J., Wu, K., Marar, T. M. K., Seetha, S., Ashoka, B. N., Mahra, H. S., Bhat, B. C., Babu, V. C., Leibowitz, E. M., Hemar, S., Ibbetson, P., Mashals, E., Meištas, E., Moskalik, P., Zoła, S., Krzesiński, J., & Pajdosz, G. 2000, MNRAS, 314, 689

Wesemael, F. 1979, A&A, 72, 104

Wesemael, F., Green, R. F., & Liebert, J. 1985, ApJS, 58, 379

Wesemael, F., Liebert, J., Schmidt, G. D., Beauchamp, A., Bergeron, P., & Fontaine, G. 2001, ApJ, 554, 1118

Wesemael, F. & Truran, J. W. 1982, ApJ, 260, 807

Wickramasinghe, D. T., Hintzen, P., Strittmatter, P. A., & Burbidge, E. M. 1975, ApJ, 202, 191

Wickramasinghe, D. T. & Reid, N. 1983, MNRAS, 203, 887

Wickramasinghe, D. T. & Whelan, J. A. J. 1977, MNRAS, 178, 11

Winget, D. & Fontaine, G. 1982, in Pulsations in Classical and Cataclysmic Variable Stars, ed. J. Cox & C. Hansen (University of Colorado, Boulder), 46

Winget, D. E., van Horn, H. M., Tassoul, M., Hansen, C. J., & Fontaine, G. 1983, ApJ, 268, L33

Remerciements

Je voudrais remercier Francois Wesemael pour sa patience et son encouragement au cours de la préparation de cette rédaction. Je remercie aussi Gilles Fontaine pour l'usage de ses modèles et nos discussions aux toutes sortes des naines blanches.